DEFINING THE VASCULAR NICHE OF HUMAN ADIPOSE TISSUE ACROSS METABOLIC CONDITIONS

Ibrahim AlZaim[1,2,ψ], Mohamed N. Hassan[1,2ψ], Luca Mannino[1], Katarina Dragicevic[1,3], Marie Balle Sjogaard[1], Joseph Festa[1], Lolita Dokshokova[1], Bettina Hansen[1], Julie N. Christensen[1], Jean Farup[1,2], Lin Lin[1,2], Samuele Soraggi[4], Henrik Holm Thomsen[5,6], Ruby Schipper[7,8], Rikke Kongsgaard Rasmussen[1], Maximilian von Heesen[9], Lena-Christin Conradi[9], Carolina E. Hagberg[7,8], Joerg Heeren[10], Anders Etzerodt[1], Margo Emont[11,12], Evan D. Rosen[11-13], Lucas Massier[14], Mikael Rydén[14], Niklas Mejhert[14], Matthias Blüher[15-17], Konstantin Khodosevich[3], Bilal N. Sheikh[15-17], Niels Jessen[1,2,18], Laura P.M.H. de Rooij[19] and Joanna Kalucka[1,2,]*

[1]Department of Biomedicine, Aarhus University, Høegh-Guldbergsgade 10, 8000, Aarhus C, Denmark
[2]Steno Diabetes Center Aarhus, Aarhus University Hospital, Aarhus, Denmark
[3]Biotech Research and Innovation Centre (BRIC), Faculty of Health and Medical Sciences, University of Copenhagen, 2200 Copenhagen, Denmark
[4]Bioinformatics Research Centre (BiRC), Department of Molecular Biology and Genetics, Aarhus University, Aarhus, Denmark
[5]Department of Internal Medicine, Viborg Regional Hospital, Viborg, Denmark
[6]Department of Clinical Medicine, Aarhus University, Aarhus, Denmark
[7]Division of Cardiovascular Medicine, Department of Medicine Solna, Karolinska Institutet, Stockholm, Sweden
[8]Center for Molecular Medicine, Karolinska Institutet, Stockholm, Sweden
[9]Clinic for General, Visceral, and Pediatric Surgery, University Medical Center Göttingen, Göttingen, Germany
[10]Department of Biochemistry and Molecular Cell Biology, University Medical Center Hamburg-Eppendorf, Hamburg, Germany
[11]Division of Endocrinology, Diabetes and Metabolism, Beth Israel Deaconess Medical Center, Boston, MA, USA
[12]Broad Institute of MIT and Harvard, Cambridge, MA; USA
[13]Harvard Medical School, Boston, MA, USA
[14]Department of Medicine Huddinge (H7), Karolinska Institutet, Karolinska University Hospital Huddinge, SE-141 83, Huddinge, Sweden
[15]Helmholtz Institute for Metabolic, Obesity and Vascular Research (HI-MAG) of the Helmholtz Zentrum München at the University of Leipzig and University Hospital Leipzig, Leipzig, Germany
[16]Medical Department III – Endocrinology, Nephrology, Rheumatology, University of Leipzig Medical Center, Leipzig, Germany
[17]Medical Faculty, University of Leipzig, Leipzig, Germany
[18]Department of Clinical Pharmacology, Aarhus University Hospital, Aarhus, Denmark
[19]CeMM Research Center for Molecular Medicine of the Austrian Academy of Sciences, Lazarettgasse 14, AKH BT 25.3, 1090, Vienna, Austria

[ψ] These authors contributed equally to this work.

* Editorial correspondence: Joanna Kalucka, PhD
Department of Biomedicine
Aarhus University
Høegh-Guldbergsgade 10
8000 Aarhus C, Denmark
tel: 0045 52 16 98 17
e-mail: joanna.kalucka@biomed.au.dk

INTRODUCTION

Adipose tissue physiology and homeostasis depends on a healthy vascular network. Vascular malfunction is a hallmark of obesity, and vascular endothelial dysfunction, in particular, precipitates metabolic diseases, including obesity and type two diabetes[1]. Although single-cell transcriptomics approaches have defined atlases of human white adipose tissue (WAT) cells[2-8], the associated adipose vascular cells remain relatively undefined[9]. Specifically, there is limited information on their heterogeneity and function, and roles in metabolic disease. To address this gap, we created a single-cell transcriptome atlas of human subcutaneous adipose tissue (SAT), comprising nearly 70,000 vascular cells from 65 individuals. We identified eight adipose endothelial cell (AdEC) populations, comprising seven canonical subtypes and a previously undescribed, heterogeneous population we named sub-AdECs. Sub-AdECs exhibit gene signatures characteristic of multiple cell types, including mesenchymal, adipocytic, and immune cells, suggesting they possess diverse properties and identities. Furthermore, we compare the transcriptomes of vascular cells from individuals living with or without obesity and type two diabetes and find metabolic disease-associated inflammatory and fibrotic transcriptomic patterns. The atlas and accompanying analyses establish a solid foundation for future investigations into the biology of vascular cells within WAT and their contributions to metabolic diseases.

RESULTS

AN INTEGRATED SINGLE CELL ATLAS OF HUMAN SAT VASCULAR CELLS REVEALS A HIGH DEGREE OF HETEROGENEITY

Despite the critical role of vascular cells in regulating the expansion and reduction of adipose tissue mass during health and disease[1], a detailed mapping of their variety within adipose tissue is lacking[9]. To obtain a comprehensive profile specifically of vascular cell types in human adipose tissue, we used single nucleus RNA sequencing (snRNA-seq), as previous reports have indicated a higher prevalence of vascular cells in snRNA-seq compared to single cell (sc)RNA-sequencing datasets[7,8]. We performed snRNA-seq on > 120,000 nuclei from subcutaneous adipose tissue (SAT) obtained from biopsies of 14 donors with a wide range of body mass index (BMI) and metabolic conditions (including donors living with and without obesity and type two diabetes). To strengthen our analysis, we combined our new dataset with seven publicly available scRNA-sequencing and snRNA-seq datasets from human SAT[2-8] to construct an integrated atlas (Extended Data Fig. 1a–c) (see *Methods* section). The atlas comprises 329,774 cells from 65 donors in the eight datasets and includes the three metabolic conditions: non-obese controls, obese and obese-diabetic (Extended Data Fig. 1c–e).

By annotating cellular populations based on their expression of canonical marker genes, we identified nine distinct cell populations, including all the major populations in human SAT reported previously[7,8] (Extended Data Fig. 1f). Of note, most vascular cells (over 60%) were identified in the snRNA-seq datasets (Extended Data Fig. 1e,g). While providing insights into the heterogeneity of vascular cells[2-8], previously published scRNA-seq datasets of human SAT do not provide a comprehensive view of the cell populations constituting the vasculature.

To gain insight into the diversity specifically of vascular cells in human SAT, we refined our transcriptome analysis to focus on AdECs (cells expressing *CDH5, PECAM1, ERG*), adipose lymphatic endothelial cells (AdLECs: cells expressing *PROX1, CCL21, MMRN1*) and mural cells, which are the smooth muscle cells and pericytes of the vasculature (cells expressing *MYH11, ACTA2, TAGLN*) (Extended Data Fig. 1f). By subsetting and re-clustering these vascular cell types, we could delineate ten well-defined populations of cells exhibiting distinct canonical marker gene signatures: eight endothelial cell populations (including arterial, venous, capillary and lymphatic cells) and two mural cell populations (including vascular smooth muscle cells and pericytes) (Fig. 1a,b and Extended Data Fig. 2a). These populations contained cells from all eight datasets, the three metabolic conditions, and most donors.

We first focused on the venous AdEC populations, defined by their expression of the pan-venous marker gene *ACKR1*[10], which play significant roles in maintaining adipose tissue homeostasis and supporting its metabolic functions. Using our integrated atlas, we identified three distinct venous AdEC populations (Fig. 1b,c(i)). The first, which we refer to as the canonical venous AdEC population V1, was characterized by the expression of *TLL1* and *ELOVL7* (Fig. 1b). The second, V2, was notable for its expression of genes encoding leukocyte adhesion molecules (*ICAM1, VCAM1, SELE*, and *SELP*)[11,12] (Fig. 1b,c(ii)). The third, which we refer to as the capillary venous AdEC population V3, was distinguished by its expression of *PLVAP* and *CD74* (Fig. 1b,c(iii)). *ACKR1*, *VCAM1*, and *ICAM1* encode proteins that facilitate immune cell recruitment to the vascular wall and infiltration into the adipose tissue[11]. Thus, their expression by the venous AdEC populations is pertinent to the function of veins as the site of immune cell infiltration[13].

We next analyzed capillary AdEC populations, defined by their expression of the pan-capillary marker gene *RBP7* (Fig. 1b,c(iv)). Adipose capillary AdECs are highly adapted to the tissue microenvironment and have been shown to modulate the handling of lipids by the adipose tissue and may thus play an important role in obesity[3]. By mining our integrated atlas, we identified two distinct capillary AdEC populations: canonical capillary AdECs (C1; expressing *RGCC* and *CA4*) and interferon-activated capillary AdECs (C2; expressing *IFITM2* and *IFI27* at levels similar to those in population V3) (Fig. 1b,c(v)). Both C1 and C2 populations expressed *FABP4*, *GPIHBP1*, and *CD36* (Fig. 1c(vi,vii), which encode proteins implicated in lipid transport and processing (Fig. 1c(vi–viii)). The C2 and V3 AdEC populations had transcriptomes typical of the interferon response, with high expression of *CD74*, *HLA* genes, *IRF3*, and *ISG15*[11] (Extended Data Fig. 2b). This suggests their role as non-professional antigen-presenting cells, as previously described for endothelial cells[13].

We further used the integrated dataset to evaluate arterial AdECs, and identified a single population, Ar, expressing *GJA5* and *NEBL*[14]; (Fig. 1b,c(ix)), and a single lymphatic AdLEC population, L, expressing *PROX1* and *MMRN1*; (Fig. 1b). Additionally, we defined two populations of mural cells: pericytes (P; expressing *INPP4B* and *PDGFRB*; Fig. 1b and Extended Data Fig. 2c), and vascular smooth muscle cells (VSMCs) (SM; expressing *MYH11* and *MYOCD*; Fig. 1b) and confirmed the presence of the marker proteins NG2 (encoded by *CSPG4*) and PDGFRB in pericytes, and α-SMA (encoded by *ACTA2*), MYH11, and TAGLN in VSMCs (Fig. 1c(x–xii) and Extended Data Fig. 2c).

In addition to the canonical endothelial subtypes (arteries, veins, capillaries, and lymphatics), we also identified a heterogenous AdEC population, which we call sub-endothelial AdECs (sub-AdECs; S). These cells exhibited low expression of endothelial markers such as *PECAM1* and *CDH5*; intriguingly, nonetheless, they showed high expression levels of genes usually associated with fibroblast and leukocyte populations (*LAMA2*, *NEGR1*, *PDGFRA*, *PTPRC*, and *MRC1*) (Fig. 1b). We confirmed the presence of sub-AdECs (expressing NEGR1, PDGFRA, and CD45 as well as endothelial cell-specific proteins) in SAT using both immunohistochemistry and flow cytometry (Fig. 1d and Extended Data Fig. 2c).

To investigate the putative functions of the various endothelial cell populations, we combined data of AdECs from the same vascular bed (e.g. venous: V1, V2 and V3 and capillary C1 and C2), in order to define functionalities specific to each vascular bed irrespective of the metabolic condition. Jaccard similarity analysis was performed on the marker genes of the different vascular populations. Notably, the newly identified sub-AdEC population clustered close to capillary AdECs, demonstrating that there is a transcriptomic similarity between these subsets (Extended Data Fig. 2d) and suggesting a potential capillary origin for these cells. We also used gene ontology (GO) analysis to attribute putative functions to the various populations of AdECs and mural cells (Fig. 1e and Extended Data Fig. 2e). We found that venous AdECs (V1, V2 and V3 combined) expressed genes implicated in antigen presentation and positive regulation of leukocyte migration, similar to venous cells of other tissues. Capillary AdECs (C1 and C2 combined) expressed genes involved in modulating endothelial cell migration, and arterial AdECs expressed genes involved in maintenance of the endothelial barrier, reflecting their functions in other organs. In contrast, sub-AdECs expressed genes involved in extracellular matrix (ECM) remodeling and, notably, in insulin signaling, which has not been previously highlighted (Fig. 1e). This suggests that this population may be involved in ECM deposition and remodeling, as well as insulin responses, which are crucial for adipose tissue remodeling and homeostasis associated with obesity and type two diabetes. Pericytes and VSMCs, which facilitate blood flow throughout the vascular network[15], expressed genes implicated in pathways related to ECM organization and muscle contraction, consistent with this function (Extended Data Fig. 2e). We subsequently computed ECM components and regulator signatures (see *Methods*)[16], which corroborated the potential role of sub-AdECs in ECM deposition and remodeling. This was evidenced by higher scores for collagen, glycoprotein, and ECM-affiliated gene expression in these sub-AdECs compared to canonical vascular AdEC populations (Extended Data Fig. 2f).

The distinct properties of endothelial cells from veins, arteries, and capillaries are reflected in the unique transcription factors (TFs) they express. To determine the potential functions of the AdEC and mural populations we performed TF activity inference analysis, which predicts the activity of a certain TF from the expression of its putative target genes (Extended Data Fig. 2g). In all the canonical AdEC subpopulations, this analysis inferred the activity of ERG, an endothelial helix-turn-helix TF that promotes vascular stability and growth through Wnt–β-catenin signaling[17] (Extended Data Fig. 2g). In capillary AdECs and sub-AdECs, the inferred activity of the hypoxia inducible factor HIF1A was high (Extended Data Fig. 2g), indicating a response to adipose tissue hypoxia in these cells. Capillary AdECs, notably, exhibited the highest inferred activity of PPARG, which regulates fatty acid metabolism (Extended Data Fig. 2g), reflecting the high expression of lipid processing

genes in this population. Venous AdECs had the highest inferred activity of NR2F2, which is required for venous specification (Extended Data Fig. 2g); consistent with published literature[18]. Moreover, the non-canonical sub-AdECs were enriched for the inferred activity of MAFB and CEBPA, which control the sprouting of endothelial cells[19] and their barrier formation[20], respectively. sub-AdECs were also enriched for the inferred activity of the AP1 complex member BATF[21], NRF1, a TF that regulates stress-responsive gene expression, and the lymphocyte-enriched transcription factor IKZF1[22-24] (Extended Data Fig. 2g). As expected, AdLECs had the highest inferred activity of PROX1, which plays a key role in the formation of the lymphatic system[25] (Extended Data Fig. 2g). Mural cells were enriched for the inferred activities of STAT4, which is required for muscle cell migration[26], and NFATC2, a member of the NFAT (nuclear factor of activated T cells) family of TFs, which regulate genes involved in cell cycle, apoptosis, and angiogenesis[27]. Additionally, mural cells showed enrichment for the inferred activities of transcription factors with as yet undefined roles in these cells, including SOX13, TFAP2A, and NR3C1 (encoding the glucocorticoid receptor (GR)) (Extended Data Fig. 2g). Although the specific roles of SOX13 and TFAP2A in mural cells remain unexplored, studies have demonstrated that adipocyte-derived factors can regulate VSMCs *in vitro*, partly via the GR[28].

To identify vascular cell populations similar to those of human SAT in mice and pigs, which are commonly used mammalian models for metabolic disease research, we collated publicly available mouse SAT snRNA-seq[7] and pig SAT scRNA-seq[29] datasets (Extended Data Fig. 3), manually annotated the cell populations based on their expression of canonical marker genes, and subsetted vascular cells, as previously described for the human atlas (Extended Data Fig. 3a–f). Using the scmap[30] algorithm, we mapped the mouse and pig vascular populations onto the human ones, revealing key similarities and notably indicating the presence of sub-AdECs also in these species (Extended Data Fig. 3g,h). Together, these analyses indicate a greater than anticipated transcriptomic and functional heterogeneity among vascular cells in human adipose tissue, which is also recapitulated in mammalian models used to study metabolic diseases.

ADIPOSE TISSUE VASCULAR CELLS EXHIBIT DISEASE-ASSOCIATED TRANSCRIPTOMIC ALTERATIONS

Vascular deterioration is a hallmark of obesity and type two diabetes[1]. When compared with the endothelial cells of other organs, AdECs appear to be particularly vulnerable to obesity-associated dysfunction[1,31]. In our SAT atlas, we found that the relative abundance of the various AdEC populations was similar in the three different metabolic conditions, likely due to differences in vascular cell abundance across studies (Fig. 2a,b). Differential gene expression analysis comparing AdEC populations from non-obese donors with those from donors with obesity or with obesity and type two diabetes revealed common and condition-specific differences. Notably, the sub-AdEC population exhibited the highest number of differentially expressed genes (DEGs), with the majority of DEGs in this population occurring in both obesity and type two diabetes (Fig. 2c and Extended Data Fig. 4a). We used gene ontology analysis to investigate the functional relevance of these DEGs. AdEC subpopulations exhibited both upregulated and downregulated gene ontology groups, some of which were specific to a metabolic condition and others were universal (Fig. 2d,e, Extended Data Fig. 4b,c, and Extended Data Fig. 5a). The V1 population from donors living with obesity and type two diabetes upregulated genes and pathways

involved in lipid handling yet demonstrated downregulation of genes associated with cellular responses to hypoxia and reactive oxygen species (Extended Data Fig. 4b); the V2 population expressed at low levels genes regulating cell extravasation, including *ICAM1* and *SELE*, and the arterial population expressed at low levels genes related to negative regulation of vascular permeability (Extended Data Fig. 4b). These data suggest that the vascular control of immune cell extravasation may be disturbed in obesity and type two diabetes, which might precipitate adipose tissue inflammation and could be employed as a potential therapeutic strategy.

In the SAT of donors with obesity and type two diabetes, when compared to that of non-obese donors, the C1 population had reduced expression of genes implicated in promoting VSMC proliferation, suggesting reduced mural cell coverage of the microvasculature and enhanced vascular permeability[32,33] (Extended Data Fig. 4b). Pericytes and VSMCs both downregulated genes involved in cell proliferation and contraction and upregulated the expression of genes involved in ECM deposition and the response to pro-fibrogenic stimuli, resembling the synthetic VSMC phenotype commonly described in atherosclerosis[34] (Extended Data Fig. 4b). Together, these data support a compromised angiogenic response and an overall vascular dysfunction, two hallmarks of obesity and type two diabetes.

Gene ontology analysis also indicated that sub-AdECs are involved in cytokine responses, antigen presentation, and leukocyte-mediated inflammation in obesity and type two diabetes (Fig. 2d,e). Furthermore, downregulated expression of genes involved in lipid processing and storage in sub-AdECs, together with those involved in cellular junctions and vascular processes, reinforces the association of endothelial dysfunction with metabolic disease (Fig. 2d,e). The analysis also indicates that sub-AdECs upregulate genes involved in both the response to type II interferon and the positive regulation of leukocyte activation in both conditions (Fig. 2d), suggesting that these cells might participate in immune processes.

We used TF activity inference analysis to determine the TF activities that were either upregulated or downregulated in metabolic disease (Fig. 2f). This analysis inferred increased activity of SREBP-1 in V1, C1, and arterial AdECs specifically in donors living with obesity and type two diabetes. SREBP-1 plays a pivotal role in upregulating expression of genes encoding lipogenic enzymes in response to metabolic changes[35] and is also activated in vascular endothelial cells experiencing disturbed flow[36]. V1, V2, and C2 AdECs exhibited increased inferred activity of TEAD4[37], and links endothelial nutrient acquisition to its angiogenic capacity. Furthermore, sub-AdECs of donors living with type two diabetes showed increased activity of RBPJ (a transcriptional regulator of Notch signaling[38]), BATF (an immune-responsive TF component of the pro-inflammatory AP1 complex[21]), and GABPA (previously predicted to play a pro-angiogenic role in endothelial cells[19]; Fig. 2f). Notably, in V1 and sub-AdECs, the inferred activity of SRF, which is important for sprouting angiogenesis and the maintenance of vessel integrity[39,40], was downregulated (Fig. 2f). Collectively, these data reveal that the vascular niche within human SAT is extensively altered under disease conditions, which supports a key role in the pathogenesis of metabolic diseases.

VASCULAR CELL POPULATIONS ARE IMPLICATED IN INTERCELLULAR COMMUNICATION IN METABOLIC HEALTH AND DISEASE

AdECs have been shown to communicate with other cellular components of the adipose tissue as well as distant organs in different pathological settings[7,38,41]. Importantly, accumulating evidence suggests that adipose vascular cells engage in intercellular communication that maintains adipose tissue homeostasis and possibly contributes to metabolic disease development[42]. To investigate the extent and types of intercellular communication in the human SAT atlas, we used differential connectome analysis. This analysis inferred an increased number of intercellular interactions and increased interaction strength in donors with obesity compared with non-obese donors (Fig. 3a). The seemingly increased signaling in obesity was mediated mainly by adipocytes and preadipocytes, adipose stem and progenitor cells (ASPCs), and sub-AdECs (Fig. 3b and Extended Data Fig. 5b). Obesity was associated with a general increase in the number and strength of interactions between adipocytes and preadipocytes and the endothelial populations, however, sub-AdECs appeared to dominate these interactions (Extended Data Fig. 5b). This is consistent with a previous report indicating increased interactions between adipocytes and endothelial cells in the SAT of donors with obesity[7]. Of note, and in contrast to the analysis in obesity, there were decreased number of interactions and interaction strength in type two diabetes compared to the non-obese condition (Fig. 3a). Similarly, interactions of adipocytes and ASPCs with vascular cells appeared to dominate intercellular interactions in obesity compounded by type two diabetes (Extended Data Fig. 5b).

More in-depth analyses of these intercellular interactions identified conserved and context-specific signaling pathways in both obesity and type two diabetes (Fig. 3c). Specifically, signaling through the vascular endothelial growth factor (VEGF) pathway was reduced in obesity and further in type two diabetes. This suggests a role for dysregulated VEGF signaling in the obese adipose tissue. Signaling through the adipokine visfatin and epidermal growth factor (EGF) pathways was specific to non-obese donors. Additionally, signaling through the transforming growth factor beta (TGFß) pathway was specific to obesity, and signaling through the bone morphogenic protein (BMP) growth factor pathway was upregulated in both obesity and obesity compounded by type two diabetes (Fig. 3c). VEGF promotes adipose tissue angiogenesis[43,44], whereas pronounced TGFß signaling halts the angiogenic response to adipose tissue expansion[44]. This suggests that the endothelium of the adipose tissue is highly responsive to angiogenic stimuli, and that angiogenic signaling is disease dependent.

To study the intercellular interactions specifically of the sub-AdECs – the endothelial cell population that showed the most significant increase in both the number and strength of interactions in obesity and type two diabetes – to gain further insights into their function, we used ligand-receptor analysis (Fig. 3d and Extended Data Fig. 5c). In obesity, sub-AdECs had reduced visfatin (NAMPT) signaling through the NAMPT–ITGA5-ITGB1 and NAMPT–INSR signaling pathways (Fig. 3d). The function of visfatin signaling in adipose tissue is poorly understood. However, plasma visfatin and its mRNA levels in SAT are reduced in obesity[45]. Visfatin expression is enhanced by inflammatory conditions[46]. It promotes the proliferation of human umbilical vein endothelial cells

(HUVECs) and their formation of tubes in culture, and enhances their expression of the VEGF receptor VEGFR2[47]. This suggests that reduced visfatin signaling in obese adipose tissue promotes obesity-associated reduction in vascular density.

Sub-AdECs from donors with obesity had reduced signaling through the semaphorin-3a/c–neuropilin-1–plexin-A2/4 ligand–receptor pathway (Fig. 3d). Endothelial semaphorin-3 (SEMA3) promotes vascular migration and guidance during vasculogenesis and sprouting angiogenesis, whereas non-endothelial SEMA3 promotes vascular remodeling[48]. This implicates reduced endothelial SEMA3 signaling in the dampened angiogenic capacity of the obese adipose tissue. In other organs and tissues, SEMA3 modulates communication between the nervous system and the vasculature[49]. Whether it also does so in adipose tissue merits further investigation. Sub-AdECs, moreover, had concomitantly upregulated TGFß and BMP signaling in obesity, supporting their involvement in ECM deposition and organization and suggesting a role in tissue fibrosis (see Fig. 1e).

To demonstrate the potential translational impact of our SAT-vascular atlas, we investigated whether any of the differentially expressed protein-coding genes in human SAT vascular cells represented potential drug targets in obesity and type two diabetes (*see Methods*). This analysis identified *IFITM1* in the V3 population, *CD74*[50] and *HLA-B*[51] in the C2 population, and *PCSK5*[52] in arterial AdECs, among others, as potentially promising druggable targets (Fig. 3e). Moreover, we used single-cell disease relevance score (scDRS; an approach that links scRNA-seq with polygenic disease-associated genes implicated by genome-wide association studies[53]) to identify the enrichment of genes associated with metabolic and cardiovascular diseases in the vascular cell subpopulations. This approach associated specific vascular populations with traits pertaining to metabolic and cardiovascular diseases (Fig. 3f). Particularly, the clusters exhibiting the interferon-response phenotype appear to associate with traits related to measures of cholesterol and glucose homeostasis (Fig. 3f).

Collectively, these analyses support the notion that certain populations of vascular endothelial cells are highly relevant to metabolic disease, displaying altered intercellular interactions and expressing druggable gene products that might be targeted therapeutically.

SUB-ENDOTHELIAL CELLS EXHIBIT SIGNATURES TO MODULATE INFLAMMATION AND FIBROSIS IN METABOLIC DISEASES

In our SAT human atlas, sub-AdECs comprised almost one third of all AdECs and appeared to heterogeneously express marker genes particular to other cellular populations (such as *PTPRC*, *PDGFRA*, and *NEGR1*) (Fig. 1b). This inevitably contributed to the heterogeneity of the biological processes implicating sub-AdECs in immune-regulatory processes, ECM remodeling, and lipid handling (Fig. 1e, Fig. 2d,e, and Extended Data Fig. 2f). To gain insights into the diversity of cells that comprise sub-AdECs, we subsetted and re-clustered sub-AdECs and analyzed their expression of distinct marker gene signatures. This analysis revealed seven subpopulations of sub-AdECs common to the eight datasets and the three metabolic conditions (Fig. 4a,b and Extended Data Fig. 6a,b).

These subpopulations expressed pan-endothelial marker genes, albeit to a lower extent than *bona fide* AdEC populations, in addition to the mesenchymal marker genes *CD44* and *ZEB2* (Extended Data Fig. 6c). This suggests that sub-AdECs might arise from distinct endothelial populations through a partial endothelial-to-mesenchymal transition (EndMT), which may contribute to AdEC heterogeneity and plasticity. EndMT is important during early stages of heart development (for creating the structures known as endocardial cushions) and for the development of the lung blood circulation. In adults, however, it may play a role in vascular diseases such as atherosclerosis, pulmonary arterial hypertension, and cerebral cavernous malformation[54]. Indeed, when we subjected primary human AdECs to pro-inflammatory and pro-fibrotic stimuli known to trigger EndMT[55], we saw a profound downregulation of endothelial marker genes and a marked upregulation of mesenchymal genes (Extended Data Fig. 6c,d). This suggests that sub-AdECs are poised to express genes typically dormant in ECs, possibly explaining their plasticity.

Sub-AdEC subpopulations included **a**ctivated **v**ascular AdECs (AV; expressing *VWF* and *MECOM*), **m**esenchymal-like AdECs (M; expressing *PDGFRB* and *RGS6*), **f**ibro-**a**dipogenic **p**rogenitor (FAP)-like AdECs (expressing *KAZN* and *DCN*, and *NEGR1*), and **a**dipocyte-like AdECs (A; expressing *PCLO* and *PLIN1*; Fig. 4b), suggesting that some subpopulations of sub-AdECs might have an adipogenic fate *in vivo*. Indeed, recent single cell transcriptomics data suggested the adipogenic potential of a subpopulation of the vascular endothelium[8], and a vascular origin of adult adipocytes has been proposed previously[56-58]. Moreover, we demonstrated experimentally the downregulation of the endothelial cell marker CD144 (VE-Cadherin, encoded by *CDH5*) and the concomitant emergence of PLIN1-coated lipid droplets in the vascular sprouts of human adipose tissue organoids after induction of adipogenesis[59] (Fig. 4c). To validate these sub-AdEC subpopulations, we demonstrated histochemically the expression of PDGFRB protein in mesenchymal-like endothelial cells, KAZN and DCN in FAP-like endothelial cells, and PCLO in adipocyte-like endothelial cells in human adipose tissue (Fig. 4c,d).

Sub-AdEC subpopulations also included two **my**eloid-like endothelial cell populations (My1 and My2; expressing *MRC1* and *CD163*) and a **ly**mphoid-like endothelial cell population (Ly; expressing *IL7R* and *CD247*), suggesting an immunomodulatory role of these endothelial subpopulations[13] (Fig. 4b). A similar immune cell-like endothelial cell population expressing *TYROBP* and *FCER1G* was described previously in an integrated single cell and spatial transcriptomic map of human WAT[8]. Moreover, endothelial cells undergoing EndMT and then acquiring a macrophage-like transcriptome were documented in mouse carotid arteries exposed to disturbed flow[60]. By using full-spectrum flow cytometry, we identified the myeloid-like endothelial cell populations (My1, My2) in the stromal vascular fraction of human SAT that express macrophage markers CD206 and CD163, along with the lymphoid-like endothelial subpopulation (Ly) expressing the T-cell surface glycoprotein CD247. This finding validates the presence of endothelial populations with immune cell-like characteristics (Fig. 4d).

To explore the potential roles of sub-AdEC subpopulations in influencing adipose tissue biology in metabolic disease, we used differential gene expression analysis to compare the subpopulations in donors with obesity and donors with obesity compounded by type two diabetes with those in non-obese donors. This analysis

revealed common and divergent transcriptomic changes associated with the diseases (Fig. 4e and Extended Data Fig. 6e). Gene ontology analysis implicated mesenchymal-like, FAP-like, and myeloid-like sub-AdEC subpopulations in the activation of immune responses (Fig. 4f), and activated vascular and FAP-like subpopulations in ECM remodeling in obesity and type two diabetes (Fig. 4f, Extended Data Fig. 6f, and Extended Data Fig. 7a). Computation of ECM components and regulator signatures[16] demonstrated that the FAP-like and mesenchymal-like sub-AdEC subpopulations expressed at particularly high levels genes encoding collagens, ECM glycoproteins and proteoglycans, as well as ECM secreted factors and ECM affiliated proteins (Extended Data Fig. 7b). The FAP-like subpopulation and the activated vascular endothelial cells also exhibited the highest and the second highest, respectively, ECM regulator signature, implicating these two populations in ECM remodeling. In sub-AdECs from donors with obesity, the adipocyte-like subpopulation was enriched primarily in gene ontology signatures for fatty acid transport and metabolism pathways, whereas this subpopulation from donors with obesity compounded by type two diabetes was enriched for activated immune responses (Extended Data Fig. 7a). This suggests that the development of type two diabetes is possibly associated with a gain of immunomodulatory functions and a loss of adipogenic capacity in these cells. Additionally, the adipocyte-like subpopulation downregulated the expression of genes related to angiogenesis and axonogenesis in obesity (Extended Data Fig. 7a). Furthermore, the adipocyte-like subpopulation appears to have lost its ability to accumulate lipids in obesity and type two diabetes whereas the mesenchymal-like subpopulation had decreased mesenchymal traits (Fig. 4f).

To gain insight into the TFs that determine the states of sub-AdEC subpopulations, we again used TF activity inference analysis (Extended Data Fig. 8a). In obesity and type two diabetes, all sub-AdEC subpopulations had increased activity of SPI1, which was recently shown to be a key driver of EndMT[61], and RUNX2, which is known to promote endothelial cell proliferation and migration in response to changes in metabolic state[62,63]. We also identified TFs with differential enrichment of inferred activity in certain subpopulations of sub-AdECs, including GATA3, NR2C2, MEF2C, NR4A1, and NRF1, whose roles in endothelial cell plasticity and cell fate warrants further investigation. Notably, all sub-AdEC subpopulations exhibited reduced inferred ZEB2 activity in obesity and type two diabetes, possibly underpinning the transition of mesenchymal-primed endothelial cells into other terminal cellular states during metabolic disease progression.

To infer the potential origin of sub-AdECs and whether their emergence might be attributed to EndMT, we computed endothelial and mesenchymal scores in AdECs with reference to the expression level of a curated list of endothelial and mesenchymal genes, and calculated the EndMT score (see *Methods* section) (Extended Data Fig. 8b). The mesenchymal score was higher in sub-AdECs compared to the rest of the endothelial populations, reflecting a hybrid endothelial–mesenchymal state. Also, among the sub-AdECs subpopulations, activated vascular AdECs had the lowest EndMT score, and FAP-like endothelial cells the highest (Extended Data Fig. 8c). This suggests that sub-AdECs may arise from canonical endothelial populations with activated vascular AdECs being a transitionary state. Indeed, sub-AdECs had gene expression signatures in common with the AdECs of other vascular beds, particularly capillary AdECs (Extended Data Fig. 7c). We therefore subsetted the C1, C2 and V3 AdEC populations, all of which had capillary gene expression signatures (Fig. 1b)), together with certain

sub-AdECs subpopulations (activated vascular, adipocyte-like, and FAP-like AdECs) and used Monocle 3[64] to map the trajectory of these cells in pseudotime by trajectory inference. This analysis indicated two divergent trajectories arising from canonical capillary AdECs through activated vascular AdECs, and bifurcating into one of two terminal cell fates: FAP-like AdECs or adipocyte-like AdECs (Extended Data Fig. 8d). This is consistent with previous studies in which adipogenic-primed precursor cells bifurcated into fibrogenic and adipogenic fates[65,66]. Also, we observed a gradual increase in the EndMT score when these cells were stratified across pseudotime, suggesting this transition is driven by EndMT (Extended Data Fig. 8d). This suggestion is supported by our observation of a decrease in the expression of endothelial marker genes specific to different vascular beds and an increase in expression of FAP-like and adipocyte-like genes along the pseudotime trajectory (Extended Data Fig. 8e). Similarly, we observed a gradual increase in the expression of genes encoding TFs implicated in EndMT (including ZEB2 and RBPJ) and the lipogenic transcription factor PPARG, and a gradual decrease in expression of the endothelial TF ERG along the pseudotime trajectory (Extended Data Fig. 8e). Collectively, these data indicate that sub-AdECs may arise from canonical AdECs and that they may play roles in modulating adipose tissue inflammation and fibrosis in metabolic diseases.

Discussion

To address the gap of knowledge regarding the diversity among adipose tissue vascular cells, we created an integrated transcriptomic atlas of human SAT vascular cells. We systematically annotated the functional characteristics of AdECs and mural cell populations, and examined how their transcriptomes and functionalities are altered in individuals with obesity and type 2 diabetes. Furthermore, we identify and characterize a previously unrecognized subpopulation of AdECs, sub-AdECs. These cells, which have a partially mesenchymal transcriptome, appear to originate from various vascular beds within the adipose tissue.

Recent studies of cells undergoing EndMT have identified cell states associated with inflammation and highlighted the role of inflammatory signaling in promoting fate conversion[67]. This inflammatory signaling appears to be a common feature of transitioning cells, whether undergoing EndMT, epithelial-to-mesenchymal transition, or endothelial-to-hematopoietic transition, and suggests it is intrinsic to endothelial cell plasticity. Furthermore, recent evidence suggests that the expression of the gene encoding CD45, a protein tyrosine phosphatase signaling molecule common to hematopoietic immune cells, in endothelial cells is sufficient to drive EndMT[68] and that CD45-expressing endothelial cells undergoing EndMT differentiate into neointimal cells to promote vascular wall remodeling in a mouse model of carotid artery ligation[69]. Further investigations are needed to determine whether the expression of inflammatory and hematopoietic markers in AdECs confers immunomodulatory functions, as has been demonstrated for endothelial cells in other systems[13,70,71].

Several studies have reported evidence that adipocytes arise from the nascent vascular sprouts of explanted adipose tissue cultured *in vitro*[57,65,72]. Although the vascular origin of adult adipocytes remains controversial[1], one recent study found a subpopulation of AdECs expressing *PDGFRA*, *CXCL14*, *APOD*, and *CFD*, suggesting they have adipogenic potential[8]. Our study identified subpopulations of sub-AdECs expressing known

adipogenic, fibroblastic, and immune cell signatures, consolidating the notion that these subpopulations have the potential to give rise to adipocyte-like and immune-like cells. The functional consequences of endothelial cells acquiring an adipogenic or an immune phenotype in adipose tissue requires further investigation, as does the question of whether these cell types arise within niches or occur evenly throughout the adipose tissue vasculature. Future studies using spatial transcriptomic approaches[8,73] will help address these fundamental questions.

Our study shows the similarity of the transcriptomes of human adipose tissue vascular cell subpopulations (including sub-AdECs) to their counterparts in mice and pigs. In comparison to the endothelial cells of other organs, the endothelial cells of adipose tissue in mice appear to be particularly vulnerable to obesity-associated metabolic disturbances[31]. Thus, mouse models of obesity will be valuable for investigating the causal role of these subpopulations in the pathogenesis of obesity. In contrast to a recently published transcriptomic atlas of white adipose tissue in a mouse model of diet-induced obesity[31], we found no proliferating AdEC populations in human SAT. However, we found computational evidence that the canonical venous and capillary AdECs in obese human subjects have a decreased proliferative capacity. This difference between mice and humans might be explained by species- and obesity duration-specific responses of AdECs to adipose expansion and tissue hypoxia. Nevertheless, findings from mice should be applied with caution to humans. In the case of pigs, a subpopulation of pig AdECs was reported to exhibit a partial mesenchymal transcriptome[29]. In humans, however, these populations are equally abundant in non-obese donors as donors with obesity and type two diabetes[74]. Indeed, the subpopulation was also found in healthy pigs[29]. It is thus plausible that these AdECs subpopulations exert homeostatic rather than pathological functions in non-obese donors.

In summary, we provide a comprehensive high-resolution atlas of the vascular cells in human SAT, including the transcriptomic signatures of nine cell populations, from which we infer their involvement in obesity and type two diabetes. We identify and characterize a novel population of adipose endothelial cells, sub-AdECs comprising subpopulations with a partial mesenchymal transcriptome that are potentially implicated in adipose tissue remodeling and immunomodulation. Also, we present a list of potential druggable targets that show disease-specific differential expression patterns in AdEC populations of particular interest. The atlas and our reported findings serve as a starting point for future efforts to investigate the biology of vascular cells, and particularly endothelial cells in adipose tissue, and to modulate their functions to curb metabolic deterioration of adipose tissue in obesity and type two diabetes.

FIGURE LEGENDS

Fig. 1: An integrated single cell atlas of human SAT vascular cells reveals a high degree of heterogeneity. a, UMAP projection of single cell transcriptomics data for 68,503 vascular cells showing the ten distinct cell populations in the human SAT atlas. **b**, Marker gene expression in each vascular cell population identified in (a). Expression of the genes indicated in red was validated in (c) and (d). Color scale: red, high expression; grey, low expression. Dot size: the percentage of cells within a cluster expressing a particular gene. **c**, *Left panels*: Immunohistochemical staining of wholemount adipose tissue for proteins encoded by the marker genes in each vascular cell population. *Right panel*: Feature plots depicting gene expression. Black arrows highlight populations with pronounced expression of particular genes. **d**, *Left panel*: Representative contour plots of flow cytometry experiments showing the presence of CD45- and PDGFRA-expressing sub-AdECs among human SAT stromovascular cells. *Right panel*: Feature plots depicting gene expression. Arrows highlight populations with pronounced expression of particular genes. **e**, Bar plots presenting five selected gene ontology (GO) terms among the most significant GO terms in venous, capillary, arterial, and sub-AdECs with the x-axis representing gene count.

Fig. 2: Adipose tissue vascular cells exhibit disease-associated transcriptomic alterations. a, UMAP projection of the vascular cells in the human SAT atlas with the indicated metabolic conditions. **b**, The proportion of each vascular cell population occurring in each metabolic condition. **c**, Venn diagrams showing the overlap of significantly differentially expressed genes in each vascular cell population in the Non-obese vs. Obese, Non-obese vs. Obese diabetic, and Obese diabetic vs. Obese comparisons. **d**, Radar plots depicting common upregulated and downregulated GO terms in sub-AdECs in the Obese vs. Non-obese and Obese diabetic vs. Non-obese comparisons. GO terms in bold are mentioned in the main text. **e**, Bar plots presenting five selected GO terms among the most significant upregulated and downregulated GO terms in sub-AdECs cells in the Obese vs. Non-obese and Obese diabetic vs. Non-obese comparisons with the x-axis representing gene count. GO terms in bold are mentioned in the text. **f**, Heatmaps depicting the inferred enrichment of transcription factor activity in each vascular cell population and in each metabolic condition. Transcription factors in bolded red have been highlighted in the text. Color scale: red, high expression; grey, low expression.

Fig. 3: Vascular cell populations are implicated in intercellular communication in metabolic health and disease. a, Bar plots depicting the number of intercellular interactions and their strength in each metabolic condition. **b**, Scatter plots showing the strength of the outgoing (x-axis) and the incoming (y-axis) interaction strength for each cell type in each metabolic condition. **c**, Bar plots showing the relative information flow for significant communication pathways in the three comparisons; Obese vs. Non-obese (*left panel*), Obese diabetic vs. Non-obese (*middle panel*), and Obese diabetic vs. Obese (*right panel*). The y-axis represents the significantly altered pathways. Colored pathways are enriched in a specific condition for a given comparison. Pathways highlighted in the text are bolded. The x-axis represents the relative information flow of a given pathway. **d**, Chord diagrams depicting the results of ligand–receptor analysis for significant signaling pathways in the sending (sub-

endothelial cells – sub-AdECs) and receiving cell populations in each metabolic condition. Capitalized and bolded ligand-receptor pairs have been highlighted in the text. **e**, Filtered druggable differentially expressed protein-coding targets in the vascular cells of human SAT in each metabolic condition. Ridge plots represent the expression level of specific genes in vascular populations as a factor of cell density (frequency of cells) **f**, Heatmap depicting significant associations between vascular cell types of human SAT and 17 relevant metabolic and cardiovascular traits.

Fig. 4: Sub-endothelial cells exhibit signatures to modulate inflammation and fibrosis in metabolic diseases. **a**, UMAP projection of single cell transcriptomics data for 16,658 sub-AdECs in the human SAT atlas showing seven distinct subpopulations. **b**, Marker gene expression in each subpopulation identified in (a). Color scale: red, high expression; grey, low expression. Dot size: the percentage of cells within a cluster expressing a particular gene. Expression of the genes indicated in red was validated in (c) and (d). **c**, *Right panel*: Immunohistochemical staining of wholemount adipose tissue for proteins encoded by the principal marker genes in sub-AdECs subpopulations. *Left panel*: Feature plots depicting gene expression. *Lower panels*: Immunohistochemical staining of three-dimensional differentiated human adipose tissue organoids for PLIN1 (encoded by *PLIN1*), a principal marker gene of the adipocyte-like endothelial cell population. Arrows highlight endothelial cells with pronounced expression of particular genes and proteins. **d**, *Right panel*: Immunohistochemical staining of wholemount adipose tissue or flow cytometric contour plots depicting the expression of proteins encoded by the principal marker genes in sub-AdECs subpopulations. *Left panel*: Feature plots depicting gene expression. Arrows highlight endothelial cells with pronounced expression of particular genes and proteins. In **c-d**, scale: red, high expression; grey, low expression**. e**, Venn diagrams showing the overlap of significantly differentially expressed genes in each sub-AdECs subpopulation in the three comparisons (Non-obese vs. Obese, Non-obese vs. Obese diabetic, and Obese diabetic vs. Obese). **f**, Radar plots presenting common upregulated and downregulated GO terms in sub-AdECs subpopulations in the Obese vs. Non-obese and Obese diabetic vs. Non-obese comparisons. GO terms in bold have been highlighted in the text.

Extended Data Fig. 1: Construction of an integrated single cell transcriptome atlas of human SAT allows the identification of heterogenous vascular cells. a, Schematic of workflows for the construction of the human SAT atlas and downstream analyses. **b**, UMAP projections of all the 329,774 cells in the human SAT atlas grouped by cohort either before (*Raw data*) or after integration (*Harmony*, *scVI*, *BBKNN*). The table (bottom right panel) shows the Graph LISI-, ARI-, and kBET-based evaluation of data integration methods and their overall ranking. **c**, UMAP projection of all the cells in the human SAT atlas grouped by *Cluster annotation*, *Condition*, and *Donor*. The bar in the legend represents individual donors. **d**, Violin plots depicting the number of UMIs and Genes per cell type in the human SAT atlas. **e**, UMAP projection of all the cells of the human SAT atlas split by cohort and technology (single cell (SC) and single nucleus (SN)). Bar graphs represent cell proportion as a percentage of all cells per cohort. **f**, Marker genes for each major cell population in the human SAT atlas. Color scale: red, high expression; grey, low expression. Dot size: the percentage of cells within a cluster expressing a particular gene.

g, Percentage of vascular cells per cohort split by technology. Each dot corresponds to a single cohort (n=4-5). In bar graphs, error bars represent ± s.e.m and *P* value was calculated using unpaired t test.

Extended Data Fig. 2: Transcriptomic and functional characterization of human SAT AdECs and mural subpopulations. a, Feature plots depicting the gene signatures of the different vascular cell populations in the human SAT atlas. Arrows highlight cells with pronounced gene signatures**.** Color scale: yellow, high expression; purple, low expression **b**, *Left panel*: Dot plot showing the enrichment of interferon-related genes in AdECs of the V2 and C3 clusters. *Right panels*: Immunohistochemical staining showing the expression of principal marker genes in human SAT wholemounts. Color scale: red, high expression; grey, low expression. Dot size: the percentage of cells within a cluster expressing a particular gene. Arrows highlight cells with pronounced expression of particular proteins. **c**, *Left panels*: Immunohistochemical staining showing the expression of principal marker genes in human SAT wholemounts. *Right panels*: Feature plots depicting gene expression. Black arrows highlight populations with pronounced expression of particular genes. **d**, Three-dimensional principal component analysis on the pairwise Jaccard similarity coefficients of marker genes of the different vascular cell populations in the human SAT atlas. **e**, Bar plots showing 5 selected GO terms among the most significant GO terms in lymphatic endothelial cells, pericytes, and VSMCs with the x-axis representing gene count. **f**, Violin plots showing the enrichment of matrisome gene signatures in the vascular cell subpopulations. **g**, Heatmaps showing the enrichment of inferred activity of transcription factors belonging to different transcription factor classes in endothelial cells (venous, capillary, arterial, lymphatic, and sub-AdECs) in addition to pericytes and VSMCs. Transcription factors in bolded red have been highlighted in the text. Color scale: red, high expression; grey, low expression.

Extended Data Fig. 3: Human, murine and porcine SAT vascular niches comprise equivalent cells. a, UMAP projections of single cell transcriptomics data of clusters formed by murine SAT (inguinal adipose tissue) cells and subsetted vascular cells comprising AdECs, AdLECs, and mural cells. **b**, UMAP projections of single cell transcriptomics data of clusters formed by porcine SAT cells and subsetted vascular cells comprising AdECs, AdLECs, and mural cells. **c**, Dot plot depicting the marker genes of the major cell types in murine SAT. **d**, Dot plot depicting the marker genes of the major cell types in porcine SAT **e**, Dot plot showing the top 20 marker genes of the major vascular cell types in porcine SAT. **f**, Dot plot showing the top 20 marker genes of the major vascular cell types in murine SAT. In **c-f**, color scale: red, high expression; grey, low expression. Dot size: the percentage of cells within a cluster expressing a particular gene. **g**, Violin plot showing the scmap similarity index between human vascular cell populations and those of mouse (upper panel) and pig (lower panel). **h**, Riverplots showing the relationship between human vascular clusters and those of mouse (upper panel) and pig (lower panel).

Extended Data Fig. 4: Adipose tissue vascular cells exhibit disease-associated traits reminiscent of metabolic disease-associated vascular dysfunction. a, Bar plot showing the number of significantly differentially expressed genes in each vascular cell population across three comparisons; Obese vs. Non-obese, Obese diabetic vs. Non-obese, and Obese diabetic vs. Obese. **b**, Radar plots presenting common upregulated and downregulated GO

terms in canonical AdECs and mural cell subpopulations. **c**, Bar plots showing 5 selected GO terms among the most significant upregulated and downregulated GO terms of AdECs belonging to the canonical AdECs and mural cell subpopulations in either of the two comparisons; Obese vs. Non-obese and Obese diabetic vs. Non-obese with the x-axis representing gene count. GO terms in bold have been highlighted in the text.

Extended Data Fig. 5: Sub-endothelial cells occur in non-obese donors, donors with obesity, and donors with obesity compounded by type two diabetes, exhibit metabolic disease-associated traits, and are implicated in intercellular interactions. a, Bar plots showing 5 selected GO terms among the most significant upregulated and downregulated GO terms of mural cell subpopulations in the Obese vs. Non-obese comparison with the x-axis representing gene count. **b**, Heatmaps depicting the differential number and strength of interactions in both the Obese vs. Non-obese and the Obese diabetic vs. Non-obese comparisons. Color scale: red, high expression; grey, low expression. **c**, Chord diagrams presenting the sending and receiving (Sub-AdECs) cellular populations in significant signaling pathways using ligand-receptor analysis.

Extended Data Fig. 6: Sub-endothelial cells exhibit metabolic disease-associated traits and share gene signatures of canonical vascular cells. a, UMAP projection of single cell transcriptomics data of sub-AdECs cells in the human SAT atlas grouped by *Condition*, *Cohort*, and *Donor*. **b**, Bar plot presenting the distribution of each sub-AdECs subpopulation across the three conditions and the eight cohorts. **c**, Feature plots depicting the expression of endothelial (*PECAM1*, *CDH5*, *VWF*, *CD34*) and mesenchymal (*CD44*, *ZEB2*) genes in sub-AdECs and the vascular cells of the human SAT atlas validated using an *in vitro* model of EndMT using qRT-PCR to assay the same genes (n=8-10). Color scale: red, high expression; grey, low expression. **d**, Representative Western blot of the mesenchymal genes TAGLN and CD44 in untreated (UT) and EndMT-induced primary human AdECs. **e**, Bar plot showing the number of significantly differentially expressed genes in each sub-AdECs subpopulation across the three comparisons; Obese vs. Non-obese, Obese diabetic vs. Non-obese, and Obese diabetic vs. Obese. **f**, Bar plots showing 5 selected GO terms among the most significant upregulated and downregulated GO terms of sub-AdECs subpopulations in either the Obese vs. Non-obese or the Obese diabetic vs. Non-obese comparison with the x-axis representing gene count. GO terms in bold have been highlighted in the text. In bar graphs, error bars represent $\pm$ s.e.m and *P* value was calculated using two tailed one sample t-test.

Extended Data Fig. 7: Sub-endothelial cells are possibly implicated in ECM remodeling and share gene signatures of canonical vascular cells. a, Bar plots showing 5 selected GO terms among the most significant upregulated and downregulated GO terms of sub-AdECs subpopulations in the Obese vs. Non-obese and the Obese diabetic vs. Non-obese comparisons with the x-axis representing gene count. GO terms in bold have been highlighted in the text. **b**, Violin plots showing the enrichment of matrisome gene signatures in sub-AdECs subpopulations. **c**, Feature plots depicting the gene signatures of the different canonical vascular cell populations within sub-AdECs. Arrows highlight cells with pronounced gene signatures**.** Color scale: yellow, high expression; purple, low expression.

Extended Data Fig. 8: Sub-endothelial cells exhibit an EndMT signature and possibly arise from canonical vascular cells. a, Heatmap showing the inferred enrichment of transcription factor activity in each sub-AdECs subpopulation in the human SAT atlas across the three conditions. Transcription factors in bolded red have been highlighted in the text. Color scale: red, high expression; grey, low expression. **b**, Scatter plots showing the endothelial and mesenchymal scores (sub-AdECs (S) cells highlighted with dashed line box) and bar plots depicting the EndMT score of each vascular cell subpopulation. **c**, Scatter plots showing the endothelial and mesenchymal scores and bar plots depicting the EndMT score of sub-AdECs subpopulations. **d**, UMAP projection of single cell transcriptomics data of selected vascular cell and sub-AdECs subpopulations depicting the pseudotime trajectories (Trajectory 1 and Trajectory 2). Box plot showing the occurrence of cells belonging to each cellular population across pseudotime. EndMT score of each cell arranged by pseudotime. **e**, Heatmap showing the top 50 marker genes per aggregated cluster arranged by their occurrence across the pseudotime trajectory and the variation in the expression of selected transcription factors in each cellular subpopulation across pseudotime. Color scale: red, high expression; grey, low expression.

Supplementary Fig. 1: Gating strategies for nuclei sorting and Sub-AdECs identification. a, Human subcutaneous adipose tissue (SAT) nuclei were gated based on size using the forward and side scatters and Hoechst^{+} singlets were sorted and used for 10X Genomic library preparation. **b**, Human SAT stromovascular fraction cells were first gated based on size using the forward and side scatters and live singlets were subsequently gated to identify CD45^{-}CD31^{+}PDGFRA^{+} and CD31^{+}CD34^{+}CD45^{+} cells. **c**, Human SAT stromovascular fraction cells were gated based on size using the forward and side scatters and live singlets were subsequently gated to identify CD45^{-}CD31^{+}PDGFRA^{+} and CD31^{+}CD34^{+}CD45^{+} cells. c, CD144^{+}CD31^{+}CD45^{+}CD247^{+} and CD144^{+}CD31^{+}CD45^{+}CD11b^{+}CD163^{+}CD206^{+} cells.

METHODS

Study cohort and clinical sample acquisition. Human deep subcutaneous adipose tissue samples were obtained from non-obese donors undergoing hemicolectomy, laparoscopic transabdominal preperitoneal approach, fundoplication with mesh hiatoplasty, or band-reinforced gastric bypass and obese donors undergoing elective cosmetic abdominoplasty, gastric sleeve resection, or gastric bypass surgeries at the Clinic for General, Visceral, and Pediatric Surgery of the University Medical Center Göttingen in Göttingen, Germany. Given the wide range of obesity and type two diabetes phenotypes, we used all the available clinical parameters to classify the donors. Obesity was defined based on body mass index (BMI) (kg/m^2): Non-obese donors (BMI < 30) and donors with obesity (BMI > 30). Donors were classified as having type two diabetes based on the presence of a previous history of type two diabetes and antidiabetic medication. This yielded three groups in total matched for age and BMI; non-obese (2 females/ 2 males, age: 45.75±13.27, BMI: 23.27±0.72), obese (3 females/ 4 males, age: 38±5.78, BMI: 53.22±8.94), and obese diabetic (2 females/ 1 male, age: 42±6.16, BMI: 51.3±6.16). The human samples used in the present study were obtained based on the presence of a signed consent according to the University Medical Center Göttingen institutional review board ethical approval (38/4/21).

Isolation of adipose tissue nuclei. Nuclei were isolated from human subcutaneous adipose tissue samples according to a previously published protocol with slight modification [75]. Approximately 1g of frozen human subcutaneous adipose tissue was finely minced in a petri dish on dry ice and transferred to a 15mL douncer containing 6.5mL Tween salt-Tris (TST) buffer [ST buffer (146mM NaCl (AM9759, Thermo Fisher Scientific), 10mM Tris-HCl (PH 7.5) (15567027, Thermo Fisher Scientific), 1mM $CaCl_2$ (97062-820, VWR International Ltd), 21mM $MgCl_2$ (M1028, Merck), 1mM DTT (R0861, Thermoscientific), and 0.2U/µL RNAse inhibitor (10777019, Invitrogen) containing 0.01% BSA (A7906, Sigma-Aldrich) and 0.03% Tween 20 (P1379, Sigma-Aldrich) in nuclease-free water (AM9930, Invitrogen)] on ice. Samples were homogenized using the douncer, applying 7 strokes with the loose pestle and 5 strokes with the tight pestle. Another 3mL of TST buffer was added and the homogenate was left to rest on ice for 10 minutes, during which occasional strokes were applied to ensure complete homogenization. The homogenate was then filtered through a 40µm cell strainer (76327-098, VWR International Ltd) and thoroughly washed with 9mL of ST buffer, then centrifuged at 500g for 10 minutes at 4 ºC. The nuclear pellet was washed once with 3mL ST buffer and then twice with 3mL FANS buffer (1% BSA, 1mM DTT, and 0.2U/µL RNAse inhibitor (03 335 402 001, Protector RNAse inhibitor, Roche) in RNAse free DPBS (AM9624, Invitrogen)), and was centrifuged at 500g for 10 minutes at 4 ºC after each wash. Finally, the nuclear pellet was resuspended in 750µL FANS buffer and filtered through a 40µm cell strainer prior to nuclear sorting. All solutions were sterile filtered prior to use.

Fluorescence-activated nuclear sorting. Isolated nuclei were stained with Hoechst (H3570, Thermo Fisher Scientific) and subjected to fluorescence-activated nuclear sorting (FANS) on a 4 laser FACSAria III high speed cell sorter into FANS buffer containing 2% BSA. A detailed gating strategy of nuclei is presented in Supplementary Fig. 1a. A small proportion of the sorted Hoechst-positive events were stained with propidium iodide (PI) and

counted on a Luna-FL automated fluorescence cell counter (Logos Biosystems, South Korea) and nuclei were submitted for snRNA-seq using the 10x Genomics system.

Single-nucleus RNA-sequencing. Immediately following FANS, nuclei were loaded onto the 10x Genomics Chromium controller. Libraries were prepared according to the manufacturer's instructions using the 10x Genomics Single-Cell 3' v3.1 (Chromium Next GEM Single Cell 3' Kit v3.1, 16 rxns (PN-1000268, 10x Genomics), Chromium Next GEM Chip G Single Cell Kit, 48 rxns (PN-1000120, 10x Genomics), and Dual Index Kit TT Set A, 96 rxns (PN-1000215, 10x Genomics). Libraries were sequenced on a DNBSEQ-G400 platform (MGI Tech).

Human SAT publicly available and in-house datasets processing, integration benchmarking, graph embedding, and visualization. The dataset repositories GEO, dbGaP, and EMBL-EBI were searched for scRNA-seq and snRNA-seq datasets of human SAT generated using the 10x Single Cell RNAseq and the 10x Single Nucleus RNAseq technologies. Non-obese SAT samples were ones derived from individuals with BMI < 30kg/m^2, while obese and obese diabetic SAT samples were derived from individuals without or with type two diabetes, respectively, with BMI > 30kg/m^2. FASTQ files containing raw sequencing reads were either downloaded from the appropriate repositories[2-7] or were provided by the authors[8]. Raw fastq files were processed to produce count matrices using cellranger v6.1.2 (10x Genomics) by mapping to the human GRCh38 reference genome[76]; *CellBender* (v0.2.2)[77] was used to remove empty droplets and ambient RNA. For each individual sample, the output from CellBender was read in R using the function Read10x_h5 provided by Seurat. Then a Seurat object was created with *min.cells* of 3 and *min.feautures* of 200. Ribosomal, mitochondrial, and hemoglobin genes, as well as other confounding transcripts including *MALAT1* and *NEAT1* were removed prior to downstream data processing. Outliers were removed based on the number of Unique molecular identifiers (UMIs) and genes detected per cell. A linear model was constructed based on the log of UMIs against the log of genes and outliers were removed. *DoubletFinder* (v2.0.3)[78] was applied to exclude potential doublets. All samples from all studies were merged and outliers of UMIs and genes were removed. Data was log normalized using *NormalizeData* function then multiplied by a scale factor of 10000. Top 2000 highly variable genes were selected using vst method and scaled regressing out the number of UMIs. Dimensionality reduction was performed using principal component analysis (PCA) and projected using Uniform Manifold Approximation and Projection (UMAP).

Data integration and benchmarking. Different integration methods, namely *Harmony* (v0.1.1)[79], single-cell variational inference (*scVI*) (v1.0.4)[80], and batch balanced K-nearest neighbor (*BBKNN)* (v1.6.0)[81] have been evaluated for batch effect correction.

Integration with Harmony. We used *RunHarmony* to integrate the data, with samples, cohort, and chemistry (Drop-seq and Chromium versions 2, 3, and 3.1) as covariates. The first 43 harmony components were selected for generating the UMAP and clustering was performed at different resolutions assessed by the clustree package (v0.5.0)[82].

Integration with scVI. Data was processed as previously described, then the top 2000 highly variables genes were used for integration. The Seurat object was converted into AnnData file format and processed with reticulate

package (v1.34). Function setup_anndata was applied specifying the samples, cohort, and chemistry as a batch key argument for batch correction. Then scVI model was created, trained and the latent representation was obtained. The resulted matrix was used as input to CreateDimReducObject and add the embeddings were added to the main object. The first 10 PCs were selected to construct the UMAP.

Integration with BBKNN. We used the function bbknn, with samples, cohort, and chemistry as a batch key argument. Clusters were identified using Leiden algorithm at resolution 0.1. Then ridge regression was performed over the integrated data. Then bbknn integration was repeated using leiden clusters as a confounder key, followed by PCA analysis and UMAP construction.

The assessment of the three integration approaches was carried out based on the calculation of LISI scores, kBET acceptance rates (1- rejection rate), and ARI coefficients for integration across technologies, cohorts, and samples. We estimated average LISI scores using *compute_lisi* command (v1.0)[79] by adding embeddings of the UMAPs along the metadata. kBET scores were calculated based on Pearson's chi-squared test using kBET package (v0.99.6)[83] and the different integrated reductions in the Seurat object. ARI was calculated using the *adj.rand.index* function in *pdfCluster* (v1.0.4)[84] by supplying factors of cohort, technology chemistry(Drop-seq and Chromium versions 2, 3, and 3.1 – single cell or single nucleus), or sample and the identified clusters. Guided by our benchmarking, *Harmony* integration collectively ranked the highest, and therefore it was applied for the rest of the analysis.

***Clustering, cellular annotation, and vascular cell identification*.** Clusters were identified after running *FindNeighbors* with the first 43 harmony corrected PCs and *FindClusters* in Seurat at different resolutions ranging from 0.1 to 3. To assign clusters to different cell types, *FindAllMarkers* was used with *min.pct* 0.15 *logFC threshold* 0.3 using Wilcoxon rank sum test. At resolution 0.1, *FindSubcluster* was utilized to subcluster a widely dispersed cellular population where subclusters without noteworthy gene expression differences were collapsed and only high-quality cells were retained for downstream analysis. Clusters were manually assigned to discrete cell types based on the top marker genes of each cluster and 9 distinct cellular populations were identified. Cellular populations were annotated as; adipocytes and preadipocytes (*ADIPOQ*, *AQP7*), ASPCs (*APOD*, *CXCL14*), adipose endothelial cells (AdECs) (*PECAM1*, *CDH5*), adipose lymphatic endothelial cells (ALECs) (*MMRN1*, *PROX1*), mural cells (*RGS6*, *ACTA2*), macrophages and monocytes (*MRC1*, *FMN1*), mast cells (*CPA3*, *HPGD*), B cells (*IGKC*, *BANK1*), and T and NK cells (*CXCR4*, *CD69*). High-quality vascular cells were selected and subjected to another iteration of highly variable gene selection, dimensionality reduction, data integration, and clustering analysis using the first 30 corrected PCs at resolution 0.7. The heterogenous population of sub-endothelial cells were then selected for further analysis applying the same pipeline as performed over the vascular cells, selecting the first 15 PCs and clustering at resolution 0.2. Vascular cells were scored for the expression of widely characterized vascular bed-specific and mural cell-specific gene signatures using the *AddModuleScore* function from Seurat.

Differential Expression and Gene Ontology (GO) Analysis across conditions. *FindMarkers* function was used to compare every cellular population between each two conditions at a time employing a logistic regression test with gender, cohort, and chemistry as covariates. The upregulated and downregulated genes (average log2 fold change above and below 0.5) were then used as input for the *enrichGO* function from clusterProfiler package (v4.8.3)[85]. All identified genes were used as background for GO enrichment. GO terms of deregulated genes with p adjusted values following Bonferroni correction inferior to 0.05 were considered significant. GO terms were arranged by q value and top GO terms were visualized. Top 5 GO terms unique to a specific comparison were visualized by bar plots. GO terms shared between both pairwise comparisons were represented as radar charts by calculating the average area under the curve (AUC) of each gene list per condition using *AUCell_run* from AUCell package (v1.22.0)[86]. GO terms in bold have been highlighted in the text.

Transcription factor analysis. To estimate possible transcription factors from the collected datasets, we used the top 3 confidence levels of the DoRothEA database (v1.12.0). We used the function run_mlm from decoupleR (v2.6.0)[87] to fit a multivariate linear model for each sample with setting the *min.size* to 5 genes per transcription factor. Transcription factors in bolded red have been highlighted in the text.

Murine and porcine SAT publicly available data processing and reference mapping across species. Murine snRNA-seq data generated by Emont M. et al. was downloaded from the online repository[7]. Only inguinal samples were selected for further analysis. Murine data was processed as previously described. Briefly, ribosomal and mitochondrial genes, *Malat1* and *Neat1*, in addition to hemoglobin genes were removed. Datasets were filtered out for outliers based on the number of UMIs and genes for each cell. Linear model was constructed and only residuals of more than -0.5 were kept. Then data integration with harmony was performed over the samples, choosing 30 harmony components, and clustered using the Louvain algorithm at resolution 0.5. High-quality vascular cells were selected and processed as mentioned before for the human data with the top 30 PCs at resolution 0.5. Porcine scRNA-seq data generated by Wang F. et al. was downloaded from the online repository[29]. Subcutaneous adipose tissue cells were retained followed by highly variable gene selection and dimensionality reduction. The first 25 PCs were selected to construct the UMAP, and clustering was performed at different resolutions, later evaluated with clustree and resolution 0.3 was chosen. Vascular cells were selected, highly variable genes recalculated and the first 19 PCs were used for UMAP and clustering at resolution 0.3. Reference mapping was performed using scmap (v1.22.3)[30] package setting *nFeatures* to 5000 genes. We used the *scmapCluster* algorithm setting the human dataset as reference, and either the murine or the porcine datasets as query with threshold 0.1. Data was visualized using the *getSankey* function and the resulting table was used to evaluate the scmap similarity index.

Jaccard Similarity Analysis. Clusters of endothelial cells belonging to a specific vascular bed were combined. Marker genes were calculated for each cell type per condition using the Seurat pipeline. Then the top 100 markers for each cell population were selected for pairwise Jaccard similarity coefficients calculation. The Jaccard coefficient is the size of intersection divided by the union sets size.

Pseudotime trajectory analysis. Trajectory inference was performed using the monocle3 package (v1.3.1)[64]. Briefly, certain populations of endothelial cells were extracted, data was normalized, top variable genes were selected, scaled and dimensions were reduced by PCA using default parameters. Batch effect was removed using harmony and plotted in 2-dimensional space using UMAP with the significant corrected harmony components. The Seurat object was transformed into a cell data set object and the rest of monocle3 pipeline was performed including *cluster_cells*, *learn_graph*, *order_cells* and *graph_test* for differential gene expression across pseudotime using morans test statistic. Differentially expressed genes changing across pseudotime with q-value exceeding 0.05 were filtered out. Significant differentially expressed genes were aggregated for each cell type using *aggregate_gene_expression* and the top 50 genes per cluster were visualized using the package pheatmap v1.0.12. Selected transcription factors, which expression changed across pseudotime were visualized using ggplot2 (v3.4.4) and their expression was smoothed using loess regression.

Computation of the Endothelial, Mesenchymal, and EndMT scores. Endothelial and Mesenchymal scores were calculated as previously described for epithelial-to-mesenchymal transition (EMT)[88]. Briefly, a list of endothelial and mesenchymal markers was compiled through manual curation of the literature, as follows:

- Endothelial genes: *PECAM1*, *CDH5*, and *VWF*.
- Mesenchymal genes: *ACTA2*, *FAP*, *S100A4*, *AIFM2*, *COL1A1*, *COL3A1*, *TWIST1*, *ZEB2*, *SNAI1*, *SNAI2*, *SMAD2*, *SMAD3*, *SMAD4*, *YAP1*, *KDM4B*, *MAPK8*, *MAPK14*, *TGFB1*, *TGFB2*, *TGFB3*, and *TGFBR1*.

EndMT scores for each endothelial cell was computed by subtracting the average RNA-seq z-scores of the endothelial marker genes from the average RNA-seq z-scores of the mesenchymal marker genes. Endothelial and mesenchymal scores were visualized using scatter plots and EndMT scores were scaled and visualized using boxplots.

Single-cell Disease Relevance Score (scDRS). scDRS was used to evaluate polygenic disease enrichment of human SAT vascular cell subpopulations as previously described[53]. Briefly, the publicly available Genome-wide association studies (GWAS) summary statistics of 74 diseases and traits (average N=346.000) were downloaded, and relevant traits were selected for downstream analysis. Statistical significance was determined by generating thousand sets of cell-specific raw control scores of Monte Carlo samples of matched control gene sets where the gene set size, mean expression, and expression variance of disease-relevant genes were matched. Raw disease and control scores of each cell were then normalized and cell-level p-values were computed based on the empirical distribution of the pooled normalized scores.

Identification of druggable targets in vascular cells. To identify potential druggable targets in the vascular cells in obesity and type two diabetes, we performed a series of filtering steps on genes tested for differential expression in the Obese vs. Non-obese and Obese diabetic vs. Non-obese comparisons. For each cell population, we identified genes with significant differential expression and only retained protein coding genes that exhibited a strong effect (absolute value of fold change > 1) in either comparison with expression detected in at least 25% of cell comprising each population. We then annotated these genes by whether they were found in the

druggable genome database based on Finan et al.[89] and only retained genes that exhibited cell-type specificity (based on the calculation of AUC) with AUC > 0.7. Druggable targets in each vascular population were then visualized using ridge plots.

Connectome analysis. Differential ligand-receptor analysis was performed using the package *CellChat* (v1.6.1)[90]. Briefly, single dataset connectome analysis was performed individually on obese, obese diabetic and non-obese cells using "Secreted signaling" data from the CellChatDB database and the functions *identifyOverExpressedGenes*, *identifyOverExpressedInteractions* and *computeCommunProb*. Communications in less than 10 cells were filtered out. Next, *computeCommunProPathway* and *aggregateNet* were used and connectome analyses comparing different datasets (obese or obese diabetic and non-obese) were carried out. For each pairwise comparison, individual CellChat objects were merged using *mergeCellChat* to calculate differential interactions through *compareInteractions* and *netVisual_diffInteraction* functions. To visualize the incoming and outgoing cellular populations in 2D space, *netAnalysis_signalingRole_scatter* and *netAnalysis_signalingChnages_scatter* functions were used. The results were visualized using heatmaps, circular diagrams and bar plots.

Isolation of human adipose tissue stromovascular fraction and endothelial cells. Human adipose tissue endothelial cells were isolated from fresh human adipose tissue according to a previously published protocol with slight modifications[75]. Human deep subcutaneous adipose tissue samples were obtained as described above at the Department of Internal Medicine, Viborg Regional Hospital, Viborg, Denmark according to the scientific ethics committee for region central Jutland approval (1-10-72-312-20) and the presence of a signed donor consent. Adipose tissue was cut into small pieces and digested for 30 minutes at 37 ºC in supplemented KnockOut™ DMEM-based digestion buffer (10829018, Gibco) containing 1% Penicillin/Streptomycin (15140122, Thermo Fisher Scientific), 2x Antibiotic-Antimycotic (15240062, Thermo Fisher Scientific), 1mM Sodium Pyruvate (11360070, Gibco), 1x MEM Non-essential amino acids (11140035, Gibco), 2mM L-glutamine (25030024, Thermo Fisher Scientific), and 1x Endothelial Cell Growth Factor supplements (ECGS/heparin) (C-30120, PromoCell) in addition to 0.1% Collagenase I (17100017, Thermo Fisher Scientific), 0.25U/mL Dispase (17105041, Gibco), and 7.5mg/mL DNAse I (D4527, Sigma-Aldrich). The solution was then filtered through a 100µm cell strainer and allowed to rest. The floating fat layer was removed, and the reaction was stopped with PBS-based wash buffer containing 0.5% BSA (A7906, Sigma-Aldrich) and 2mM EDTA (E177, VWR). The solution was then spun down at 300g for 7 minutes and the pellet was either resuspended in wash buffer for downstream endothelial cell isolation or was resuspended in 1ml StemMACS™ Cryo-Brew solution (130-109-558, Miltenyi Biotec) and frozen until later use. For downstream endothelial cell isolation, cells were washed twice with wash buffer and then incubated with CD45 human Microbeads (130-045-801, Miltenyi Biotec) for 20 minutes. Cells were then washed with wash buffer and passed through an activated MS column (130-042-201, Miltenyi Biotec). The column was washed three times. The eluted solution was centrifuged, and cells were incubated with CD31 human Microbeads and FcR Blocking Reagent (130-091-93, Miltenyi Biotec) according to the manufacturer's protocol for 20 minutes. Cells were washed and passed through an activated MS column as previously described. Magnetically labeled cells were immediately flushed out by firmly pushing the plunger in the column. Isolated

cells were plated on 0.1% gelatin-pre-coated culture flasks in supplemented Endothelial Cell Growth Medium 2 (ECGM2) (C-22011, PromoCell) containing 2x Antibiotic/Antimycotic at 37 ºC, 5% CO2, and were passaged at confluence. Cells were used in single-donor cultures and between passages 1 and 5.

Human adipose tissue organoid culture and immunostaining. Primary human SVF cells were used to form human adipose tissue organoids as previously described[59]. Briefly, primary human SVF cells (Lonza Bioscience, Switzerland) were seeded in a 96-well ultra-low attachment plate with a round bottom (CLS7007, Corning) at 10,000 cells per well in EGM-2 (CC-3162, Lonza) in a 5% CO2 humidified incubator at 37 ºC. On day 6 (d6), the formed spheroids were embedded in growth factor-reduced Matrigel (11553620, Corning) and maintained in EGM-2 until d10. On d10, half of the cell culture media was replaced with 2x concentrated preadipocyte growth medium (PGM-2, PT-8002, Lonza) and media was changed on d15 and d20. Spheroids were harvested on d10, d15, d20, and d25, fixed with 4% PFA for 30 minutes, and then washed and maintained in PBS until stained. Spheroids were incubated in blocking buffer (3% BSA 1% Tween-20 in PBS) for 2 hours and then incubated with primary antibodies (goat anti-mouse VE-Cadherin (AF1002, R&D systems) (1:100) and rabbit anti-Perilipin 1 (PA5-81240, Invitrogen) (1:100) overnight at 4 ºC. Spheroids were then washed and incubated with BODIPY 493/503 (D3922, Invitrogen), and 1:100 donkey anti-rabbit Alexa Fluor 647 (A-31573, Invitrogen) and donkey anti-goat Alexa Fluor 568 (A11057, Invitrogen) for two hours at room temperature. Spheroids were then washed and counterstained with Hoechst (1:500) prior to mounting.

In vitro induction of EndMT. Primary human AdECs were cultured in ECGM2 supplemented with endothelial cell growth supplement on 0.1% gelatin coated culturing flasks in a 5% CO2 humidified incubator at 37 ºC. Media with supplements was replaced three times per week and cells were passaged at confluence by washing once with PBS, trypsinization, and centrifugation at 500g for 5 minutes. For the induction of EndMT, AdECs were seeded at a density of 150,000 cells/well in 12-well plates. The next day, supplemented ECGM2 was replaced with a 1:1 media comprising ECGM2 and M-199 (22350078, Gibco) supplemented with endothelial cell growth supplement. Cells were then either treated with a combination of TGF-β2 (100-35B, PeproTech) (10ng/mL), TGF-β1 (100-21, PeproTech) (10ng/mL), and IL-1β (200-01B, PeproTech) (10ng/mL), or their respective vehicles according to the manufacturer's instructions. Media and treatment were replenished every other day and cells were harvested seven days following EndMT induction.

RNA isolation, cDNA synthesis, and Quantitative RT-PCR. Total RNA was extracted using TRI Reagent (T9424, Sigma-Aldrich) and converted to cDNA using the iScript cDNA synthesis kit (1708891, Bio-Rad). RNA expression analysis was performed by quantitative RT-PCR (LightCycler 480 system, Roche) using primer sets (Merck Millipore) designed with the Primer Designing Tool from NCBI (https://www.ncbi.nlm.nih.gov/tools/primer-blast/). For comparison of gene expression between conditions, expression levels (normalized to the geometric mean of the housekeeping genes GAPDH and ACTB) were expressed relative to control conditions via ΔCT method.

***Protein isolation and immunoblotting*.** Cell lysates were prepared in RIPA lysis buffer (89900, Thermo Fisher Scientific) with protease and phosphatase inhibitors (78440, Thermo Fisher Scientific) inhibitors. Lysates were then centrifuged at 4°C for 10 minutes at 12,000 g and supernatant was used for analysis. Protein content was measured using Pierce BCA Protein Assay Kit (23227, Thermo Fisher Scientific). Lysates were separated by SDS-PAGE under reducing conditions, transferred to a PVDF membrane (1704157,Bio-Rad), and analyzed by immunoblotting. Primary antibodies used were rabbit anti-TAGLN (ab14106, abcam), rabbit anti-CD44 (GTX102111, GeneTex), and mouse anti-Vinculin (V9131, Sigma-Aldrich). Appropriate secondary antibodies were polyclonal goat anti-mouse immunoglobulins/HRP (P0447, Agilent) and polyclonal goat anti-rabbit immunoglobulins/HRP (P0448, Agilent). Signal was detected using the ECL system (32106, Thermo Fisher Scientific) and densitometric quantifications were done using the Fiji software (https://fiji.sc).

***Whole mount immunohistochemistry*.** Whole human subcutaneous adipose tissue samples were fixed in 4% paraformaldehyde for 24 hours before being washed and maintained in PBS at 4 ºC for a maximum of 2 weeks. Whole adipose tissue was incubated in protein blocking buffer (3% BSA and 1% Triton X-100 in PBS) for 2 hours at room temperature on a rocking platform. Subsequently, tissues were incubated in 1:100 primary antibodies diluted in protein blocking buffer overnight, washed with PBS, and incubated with 1:100 secondary antibodies or pre-labeled primary antibodies diluted in protein blocking buffer overnight. Tissues were then washed with PBS and counterstained with Hoechst (1:500) prior to mounting. The following stains and antibodies were used: BODIPY 493/503 (D3922, Invitrogen), rabbit anti-RBP7 (HPA034749, Sigma-Aldrich), rabbit anti-FABP4 (710189, Invitrogen), rabbit anti-CA4 (10472-R039, SinoBiological), rat anti-GPIHBP1 (a generous gift from Stephen G. Young, University of California, Los Angeles, USA), rabbit anti-VCAM-1 (13662, Cell Signaling Technology), rabbit anti-ACKR1 (HPA017672, Sigma-Aldrich), mouse anti-GJA5 (sc-365107, Santa Cruz Biotechnology), rabbit anti-MYH11 (ab53219, abcam), rabbit anti-alpha-SMA (19245, Cell Signaling Technology), rabbit anti-PDGFRB (MA5-15143, Invitrogen), rabbit anti-NEGR1 (HPA011894, Sigma-Aldrich), mouse anti-DCN (H00001634-M01, Thermo Fisher Scientific), rabbit anti-KAZN (PA5-56925, Invitrogen), rabbit anti-PCLO (HPA015858, Sigma-Aldrich), mouse anti-CLDN5 (35-2500, Invitrogen), mouse anti-HLA-DR (555556, BD Biosciences), rabbit anti-IRF3 (11904, Cell Signaling), rabbit anti-TAGLN (ab14106, abcam), mouse anti-NG2 (14-6504-80, Invitrogen), rat anti-PLVAP (MECA-32, DHSB), affinity purified anti-AQP1 (2353AP), rabbit anti-ISG15 (2743, Cell Signaling), recombinant human IgG1 anti-CD31-APC (130-111-354, Miltenyi Biotec), donkey anti-mouse Alexa Fluor 488 (A-21202, Invitrogen), goat anti-rat Alexa Fluor 488 (ab150157, abcam), and goat anti-rabbit Alexa Fluor 488 (A-11008, Invitrogen). Z-stack images were acquired using a LSM 900 inverted confocal microscope and analyzed using the Zeiss software.

***Flow cytometry and spectral flow cytometry*.** Human SAT stromovascular cells were thawed and resuspended in a total of 10ml ECGM2 media, spun down, and the cell pellet was resuspended in wash buffer then incubated with CD31 human Microbeads and FcR Blocking Reagent according to the manufacturer's instructions for 20 minutes. Cells were then washed with wash buffer and passed through an activated MS column. Magnetically labeled cells were immediately flushed out by firmly pushing the plunger in the column. Isolated cells were spun down, resuspended in 100ul wash buffer, and stained with Hoechst (1:500), CD45-PE-Vio770 (1:50) (130-110-

634, Miltenyi Biotec), CD31-APC (1:50) (130-111-354, Miltenyi Biotec), CD34-PE (1:50) (12-0349-41, Invitrogen), and PDGFRA-PE (1:50) (A15785, Invitrogen) for 30 minutes at 4 ºC. Cells were then washed twice with wash buffer and data were acquired on a NovoCyte 3000 flow cytometer equipped with three lasers (405nm, 488nm, and 640 nm) and 13 fluorescence detectors using the NovoExpress (v. 1.6.2) software (Agilent, Santa Clara, CA). Data analysis was carried out using FlowJo (v. 10.10.0). Detailed gating strategies of $CD45^{-}CD31^{+}PDGFRA^{+}$ and $CD31^{+}CD34^{+}CD45^{+}$ cells are presented in Supplementary Fig. 1b. For spectral flow cytometry, SAT stromovascular cells were thawed in RPMI 1640 (31870-025, Gibco) containing 100µg/mL DNAse I (100-0762, StemCell) for 15 minutes at room temperature. One million cells were then stained using Live/Dead fixable blue (L23105, Invitrogen) in 1X PBS (SH30256.01, Cytiva) for 20 minutes at room temperature. Subsequently, cells were incubated with an antibody mix (1:200 HAL-DR-BUV615 (G46-6, 751142, BD Optibuild), 1:600 CD206-BUV661 (19.2, 741641, BD Optibuild), 1:300 CD19-BUV805 (HIB19, 742007, BD Optibuild), 1:100 CD127-BV421 (HIL-7R-M21, 562437, BD Biosciences), 1:200 CD11b-BV570 (ICRF44, 301325, Biolegend), 1:200 CD3-BV605 (SK7, 563219, BD Horizon), 1:100 CCR2-BV786 (1D9, 747855, BD Optibuild), 1:50 CDH5-PE (REA199, 130-118-358, Miltenyi Biotec), 1:50 CD31-APC (REA1028, 130-111-354, Miltenyi Biotec), 1:100 CD163-R718 (Mac2-158, 568185, BD Horizon), and 1:1000 CD45-APC-Vio770 (REA747, 130-110-635, Biolegend)) containing human IgG (Privigen) and OligoBlock[91] in FACS buffer (1mM EDTA pH 8.0 (15575-038, Invitrogen), 2.5% fetal calf serum, 0.09% NaN3 (52300.0500, Ampliqon) in 1X PBS pH 7.4) at 4 degrees for 30 minutes. Finally, cells were intracellularly stained with 1:50 CD247-PerCP-eFluor710 (6B10.2, 46-247-42, Invitrogen) overnight at 4 degrees using the eBioscienceTM Foxp3/Transcription factor staining buffer set (00-5523-00, Invitrogen) according to the manufacturer's instructions. Stained, unstained, and fluorescence minus one (FMO) cells were run on an ID7000 full spectrum flow cytometer equipped with five lasers (355nm, 405nm, 488nm, 561nm, and 637nm) and 147 fluorescence detectors (SONY Biotechnologies, San Jose, CA). Unmixing was performed using UltraComp eBeadsTM Plus compensation beads (Invitrogen) and using the ID7000 Software version 2.0.2 (SONY Biotechnologies, San Jose, CA) utilizing the Weighted Least Squares Method (WLSM) algorithm for spectral unmixing. Subsequent analyses were performed in FlowJo (v. 10.10.0) using the PeacocQC[92] (v. 1.5.0). Detailed gating strategies of $VE\text{-}Cadherin^{+}CD31^{+}CD45^{+}CD247^{+}$ and $VE\text{-}Cadherin^{+}CD31^{+}CD45^{+}CD11b^{+}CD163^{+}CD206^{+}$ cells are presented in Supplementary Fig. 1c.

Data Availability. The raw sequencing data generated in this study is available at Gene expression omnibus (GEO) under the accession code GSE268904**.** Publicly available datasets were downloaded from their respective repositories. Tabula Sapiens data were retrieved from the Tabula Sapiens portal. Data from Massier et al. were obtained after contacting the authors. For questions about the incorporated datasets, the in-house dataset, or code availability, please contact the corresponding author.

Statistics. Data are represented as mean ± s.e.m of at least eight independent experiments. Statistical analysis was performed using GraphPad Prism v.10.2.2. Statistical significance between two groups was calculated using two-tailed one sample t test (for comparison to point-normalized data) or unpaired two-tailed t test with Welch correction. *P* values inferior to 0.05 were considered significant. Statistical tests used for all computational analyses are mentioned under each method. Gene ontology analysis was performed using over-representation

analysis based on hypergeometric distribution. Differential expression analysis across pseudotime was computed using Moran's I statistics. For connectome analysis, significant interactions were calculated using permutation test. For all computational analyses, *P* values were adjusted after correcting for false discovery rate using Benjamini-Hochberg and was considered significant if inferior to 0.05. For the identification of druggable genome targets, gene expression specificity was assessed based on AUC for each gene calculated using receiver operating characteristic (roc) test.

ACKNOWLEDGMENTS

This work was supported by Lundbeckfonden (R307-2018-3667), Carlsberg Fonden (CF19-0687), and Riisfort Fonden to J.K.; Novo Nordisk Foundation (NNF20OC0063268 to S.S., NNF21OC0071718 to L.L., and NNF21OC0067146 to K.K.); Swedish Research Council (#2019-02046) and Karolinska Institutet (2-189/2022 and 2020-00893) to C.E.H.; DFG-funded consortium SFB-Transregio 333, project-ID 450149205 to J.H.; and RC2 DK116691 to E.D.R. Matthias Blüher received personal honoraria from Amgen, AstraZeneca, Bayer, Boehringer-Ingelheim, Daiichi-Sankyo, Lilly, Novo Nordisk, Novartis, and Sanofi. We thank the study participants for their involvement.

COMPETING INTERESTS

The authors declare no competing interests.

REFERENCES

1 AlZaim, I., de Rooij, L. P., Sheikh, B. N., Börgeson, E. & Kalucka, J. The evolving functions of the vasculature in regulating adipose tissue biology in health and obesity. *Nature Reviews Endocrinology*, 1-17 (2023).

2 Merrick, D. *et al.* Identification of a mesenchymal progenitor cell hierarchy in adipose tissue. *Science* **364**, eaav2501 (2019).

3 Vijay, J. *et al.* Single-cell analysis of human adipose tissue identifies depot-and disease-specific cell types. *Nature metabolism* **2**, 97-109 (2020).

4 Hildreth, A. D. *et al.* Single-cell sequencing of human white adipose tissue identifies new cell states in health and obesity. *Nature immunology* **22**, 639-653 (2021).

5 Consortium*, T. S. *et al.* The Tabula Sapiens: A multiple-organ, single-cell transcriptomic atlas of humans. *Science* **376**, eabl4896 (2022).

6 Barboza, C. S. *et al.* Single-nuclei transcriptome of human adipose tissue reveals metabolically distinct depot-specific adipose progenitor subpopulations. *bioRxiv*, 2022.2006. 2029.496888 (2022).

7 Emont, M. P. *et al.* A single-cell atlas of human and mouse white adipose tissue. *Nature* **603**, 926-933 (2022).

8 Massier, L. *et al.* An integrated single cell and spatial transcriptomic map of human white adipose tissue. *Nature Communications* **14**, 1438 (2023).

9 Maniyadath, B., Zhang, Q., Gupta, R. K. & Mandrup, S. Adipose tissue at single-cell resolution. *Cell Metabolism* **35**, 386-413 (2023).

10 Thiriot, A. *et al.* Differential DARC/ACKR1 expression distinguishes venular from non-venular endothelial cells in murine tissues. *BMC biology* **15**, 1-19 (2017).

11 Kalucka, J. *et al.* Single-cell transcriptome atlas of murine endothelial cells. *Cell* **180**, 764-779. e720 (2020).

12 Li, J. *et al.* Neurotensin is an anti-thermogenic peptide produced by lymphatic endothelial cells. *Cell metabolism* **33**, 1449-1465. e1446 (2021).

13 Amersfoort, J., Eelen, G. & Carmeliet, P. Immunomodulation by endothelial cells—partnering up with the immune system? *Nature Reviews Immunology* **22**, 576-588 (2022).

14 Su, T. *et al.* Single-cell analysis of early progenitor cells that build coronary arteries. *Nature* **559**, 356-362 (2018).

15 van Splunder, H., Villacampa, P., Martínez-Romero, A. & Graupera, M. Pericytes in the disease spotlight. *Trends in Cell Biology* (2023).

16 Shao, X. *et al.* MatrisomeDB 2.0: 2023 updates to the ECM-protein knowledge database. *Nucleic Acids Research* **51**, D1519-D1530 (2023).

17 Birdsey, G. M. *et al.* The endothelial transcription factor ERG promotes vascular stability and growth through Wnt/β-catenin signaling. *Developmental cell* **32**, 82-96 (2015).

18 Trimm, E. & Red-Horse, K. Vascular endothelial cell development and diversity. *Nature Reviews Cardiology* **20**, 197-210 (2023).

19 Jeong, H.-W. *et al.* Transcriptional regulation of endothelial cell behavior during sprouting angiogenesis. *Nature communications* **8**, 726 (2017).

20 Kakogiannos, N. *et al.* JAM-A Acts via C/EBP-α to Promote Claudin-5 Expression and Enhance Endothelial Barrier Function. *Circ Res* **127**, 1056-1073 (2020). https://doi.org/10.1161/circresaha.120.316742

21 Reyes-Palomares, A. *et al.* Remodeling of active endothelial enhancers is associated with aberrant gene-regulatory networks in pulmonary arterial hypertension. *Nature communications* **11**, 1673 (2020).

22 Hoshino, A. *et al.* Gain-of-function IKZF1 variants in humans cause immune dysregulation associated with abnormal T/B cell late differentiation. *Sci Immunol* **7**, eabi7160 (2022). https://doi.org/10.1126/sciimmunol.abi7160

23 Goh, W. *et al.* IKAROS and AIOLOS directly regulate AP-1 transcriptional complexes and are essential for NK cell development. *Nature Immunology*, 1-16 (2024).

24 Boutboul, D. *et al.* Dominant-negative IKZF1 mutations cause a T, B, and myeloid cell combined immunodeficiency. *The Journal of clinical investigation* **128**, 3071-3087 (2018).

25 Potente, M. & Mäkinen, T. Vascular heterogeneity and specialization in development and disease. *Nature Reviews Molecular Cell Biology* **18**, 477-494 (2017).

26 Lv, L., Meng, Q., Ye, M., Wang, P. & Xue, G. STAT4 deficiency protects against neointima formation following arterial injury in mice. *Journal of Molecular and Cellular Cardiology* **74**, 284-294 (2014).

27 Mognol, G. P., Carneiro, F. R. G., Robbs, B. K., Faget, D. V. & Viola, J. P. d. B. Cell cycle and apoptosis regulation by NFAT transcription factors: new roles for an old player. *Cell death & disease* **7**, e2199-e2199 (2016).

28 Nguyen Dinh Cat, A. *et al.* Adipocyte-derived factors regulate vascular smooth muscle cells through mineralocorticoid and glucocorticoid receptors. *Hypertension* **58**, 479-488 (2011).

29 Wang, F. *et al.* Endothelial cell heterogeneity and microglia regulons revealed by a pig cell landscape at single-cell level. *Nature communications* **13**, 3620 (2022).

30 Kiselev, V. Y., Yiu, A. & Hemberg, M. scmap: projection of single-cell RNA-seq data across data sets. *Nature methods* **15**, 359-362 (2018).

31 Bondareva, O. *et al.* Single-cell profiling of vascular endothelial cells reveals progressive organ-specific vulnerabilities during obesity. *Nature Metabolism* **4**, 1591-1610 (2022).

32 Armulik, A., Genové, G. & Betsholtz, C. Pericytes: developmental, physiological, and pathological perspectives, problems, and promises. *Developmental cell* **21**, 193-215 (2011).

33 Holm, A., Heumann, T. & Augustin, H. G. Microvascular mural cell organotypic heterogeneity and functional plasticity. *Trends in cell biology* **28**, 302-316 (2018).

34 Basatemur, G. L., Jørgensen, H. F., Clarke, M. C., Bennett, M. R. & Mallat, Z. Vascular smooth muscle cells in atherosclerosis. *Nature reviews cardiology* **16**, 727-744 (2019).

35 Shimano, H. *et al.* Sterol regulatory element-binding protein-1 as a key transcription factor for nutritional induction of lipogenic enzyme genes. *Journal of Biological Chemistry* **274**, 35832-35839 (1999).

36 Liu, Y. *et al.* Shear stress activation of SREBP1 in endothelial cells is mediated by integrins. *Arteriosclerosis, thrombosis, and vascular biology* **22**, 76-81 (2002).

37 Ong, Y. T. *et al.* A YAP/TAZ-TEAD signalling module links endothelial nutrient acquisition to angiogenic growth. *Nature metabolism* **4**, 672-682 (2022).

38 Taylor, J. *et al.* Endothelial Notch1 signaling in white adipose tissue promotes cancer cachexia. *Nature Cancer* **4**, 1544-1560 (2023).
39 Franco, C. A. *et al.* Serum response factor is required for sprouting angiogenesis and vascular integrity. *Developmental cell* **15**, 448-461 (2008).
40 Weinl, C. *et al.* Endothelial SRF/MRTF ablation causes vascular disease phenotypes in murine retinae. *The Journal of clinical investigation* **123**, 2193-2206 (2013).
41 Monelli, E. *et al.* Angiocrine polyamine production regulates adiposity. *Nat Metab* **4**, 327-343 (2022). https://doi.org/10.1038/s42255-022-00544-6
42 Festa, J., AlZaim, I. & Kalucka, J. Adipose tissue endothelial cells: insights into their heterogeneity and functional diversity. *Current Opinion in Genetics & Development* **81**, 102055 (2023).
43 Herold, J. & Kalucka, J. Angiogenesis in adipose tissue: the interplay between adipose and endothelial cells. *Frontiers in physiology* **11**, 624903 (2021).
44 Cao, Y. Angiogenesis modulates adipogenesis and obesity. *The Journal of clinical investigation* **117**, 2362-2368 (2007).
45 Pagano, C. *et al.* Reduced plasma visfatin/pre-B cell colony-enhancing factor in obesity is not related to insulin resistance in humans. *The Journal of Clinical Endocrinology & Metabolism* **91**, 3165-3170 (2006).
46 Romacho, T. *et al.* Visfatin as a novel mediator released by inflamed human endothelial cells. *PloS one* **8**, e78283 (2013).
47 Adya, R., Tan, B. K., Punn, A., Chen, J. & Randeva, H. S. Visfatin induces human endothelial VEGF and MMP-2/9 production via MAPK and PI3K/Akt signalling pathways: novel insights into visfatin-induced angiogenesis. *Cardiovascular research* **78**, 356-365 (2008).
48 Valdembri, D., Regano, D., Maione, F., Giraudo, E. & Serini, G. Class 3 semaphorins in cardiovascular development. *Cell adhesion & migration* **10**, 641-651 (2016).
49 Wagner, J. U. *et al.* Aging impairs the neurovascular interface in the heart. *Science* **381**, 897-906 (2023).
50 Ke, K. *et al.* Increased expression of CD74 in atherosclerosis associated with inflammatory responses of endothelial cells and macrophages. *Biochemical Genetics*, 1-17 (2023).
51 Zhang, L. *et al.* Single-cell transcriptomic profiling of lung endothelial cells identifies dynamic inflammatory and regenerative subpopulations. *JCI insight* **7** (2022).
52 Suur, B. E. *et al.* Therapeutic potential of the Proprotein Convertase Subtilisin/Kexin family in vascular disease. *Frontiers in Pharmacology* **13**, 988561 (2022).
53 Zhang, M. J. *et al.* Polygenic enrichment distinguishes disease associations of individual cells in single-cell RNA-seq data. *Nature genetics* **54**, 1572-1580 (2022).
54 Xu, Y. & Kovacic, J. C. Endothelial to mesenchymal transition in health and disease. *Annual Review of Physiology* **85**, 245-267 (2023).
55 Xiong, J. *et al.* A metabolic basis for endothelial-to-mesenchymal transition. *Molecular cell* **69**, 689-698. e687 (2018).
56 Tang, W. *et al.* White fat progenitor cells reside in the adipose vasculature. *Science* **322**, 583-586 (2008).
57 Tran, K.-V. *et al.* The vascular endothelium of the adipose tissue gives rise to both white and brown fat cells. *Cell metabolism* **15**, 222-229 (2012).
58 Cattaneo, P. *et al.* Parallel lineage-tracing studies establish fibroblasts as the prevailing in vivo adipocyte progenitor. *Cell reports* **30**, 571-582. e572 (2020).

59 Ioannidou, A. *et al.* Hypertrophied human adipocyte spheroids as in vitro model of weight gain and adipose tissue dysfunction. *The Journal of Physiology* **600**, 869-883 (2022).
60 Andueza, A. *et al.* Endothelial reprogramming by disturbed flow revealed by single-cell RNA and chromatin accessibility study. *Cell reports* **33** (2020).
61 Ren, J. *et al.* Single-cell sequencing reveals that endothelial cells, EndMT cells and mural cells contribute to the pathogenesis of cavernous malformations. *Experimental & Molecular Medicine* **55**, 628-642 (2023).
62 Pierce, A. D. *et al.* Glucose-activated RUNX2 phosphorylation promotes endothelial cell proliferation and an angiogenic phenotype. *Journal of cellular biochemistry* **113**, 282-292 (2012).
63 Mochin, M. T. *et al.* Hyperglycemia and redox status regulate RUNX2 DNA-binding and an angiogenic phenotype in endothelial cells. *Microvascular Research* **97**, 55-64 (2015).
64 Cao, J. *et al.* The single-cell transcriptional landscape of mammalian organogenesis. *Nature* **566**, 496-502 (2019).
65 Yang Loureiro, Z. *et al.* Wnt signaling preserves progenitor cell multipotency during adipose tissue development. *Nature Metabolism*, 1-15 (2023).
66 Palani, N. P. *et al.* Adipogenic and SWAT cells separate from a common progenitor in human brown and white adipose depots. *Nature metabolism*, 1-18 (2023).
67 Zhang, Y., Kang, Z., Liu, M., Wang, L. & Liu, F. Single-cell omics identifies inflammatory signaling as a trans-differentiation trigger in mouse embryos. *Developmental Cell* (2024).
68 Nasim, S. *et al.* CD45 Is Sufficient to Initiate Endothelial-to-Mesenchymal Transition in Human Endothelial Cells—Brief Report. *Arteriosclerosis, Thrombosis, and Vascular Biology* **43**, e124-e131 (2023).
69 Yamashiro, Y. *et al.* Partial endothelial-to-mesenchymal transition mediated by HIF-induced CD45 in neointima formation upon carotid artery ligation. *Cardiovascular Research* **119**, 1606-1618 (2023).
70 Geldhof, V. *et al.* Single cell atlas identifies lipid-processing and immunomodulatory endothelial cells in healthy and malignant breast. *Nature communications* **13**, 5511 (2022).
71 Zeng, Q. *et al.* Understanding tumour endothelial cell heterogeneity and function from single-cell omics. *Nature Reviews Cancer*, 1-21 (2023).
72 Min, S. Y. *et al.* Human'brite/beige'adipocytes develop from capillary networks, and their implantation improves metabolic homeostasis in mice. *Nature medicine* **22**, 312-318 (2016).
73 Bäckdahl, J. *et al.* Spatial mapping reveals human adipocyte subpopulations with distinct sensitivities to insulin. *Cell metabolism* **33**, 1869-1882. e1866 (2021).
74 Whytock, K. L. *et al.* Single cell full-length transcriptome of human subcutaneous adipose tissue reveals unique and heterogeneous cell populations. *Iscience* **25** (2022).
75 Herold, J. & Kalucka, J. in *Angiogenesis* 235-250 (Springer, 2022).
76 Frankish, A. *et al.* GENCODE reference annotation for the human and mouse genomes. *Nucleic acids research* **47**, D766-D773 (2019).

77 Fleming, S. J. *et al.* Unsupervised removal of systematic background noise from droplet-based single-cell experiments using CellBender. *Nature methods* **20**, 1323-1335 (2023).
78 McGinnis, C. S., Murrow, L. M. & Gartner, Z. J. DoubletFinder: doublet detection in single-cell RNA sequencing data using artificial nearest neighbors. *Cell systems* **8**, 329-337. e324 (2019).
79 Korsunsky, I. *et al.* Fast, sensitive and accurate integration of single-cell data with Harmony. *Nature methods* **16**, 1289-1296 (2019).
80 Lopez, R., Regier, J., Cole, M. B., Jordan, M. I. & Yosef, N. Deep generative modeling for single-cell transcriptomics. *Nature methods* **15**, 1053-1058 (2018).
81 Polański, K. *et al.* BBKNN: fast batch alignment of single cell transcriptomes. *Bioinformatics* **36**, 964-965 (2020).
82 Zappia, L. & Oshlack, A. Clustering trees: a visualization for evaluating clusterings at multiple resolutions. *Gigascience* **7**, giy083 (2018).
83 Büttner, M., Miao, Z., Wolf, F. A., Teichmann, S. A. & Theis, F. J. A test metric for assessing single-cell RNA-seq batch correction. *Nature methods* **16**, 43-49 (2019).
84 Azzalini, A. & Menardi, G. Clustering via nonparametric density estimation: The R package pdfCluster. *arXiv preprint arXiv:1301.6559* (2013).
85 Wu, T. *et al.* clusterProfiler 4.0: A universal enrichment tool for interpreting omics data. *The innovation* **2** (2021).
86 Aibar, S. *et al.* SCENIC: single-cell regulatory network inference and clustering. *Nature methods* **14**, 1083-1086 (2017).
87 Badia-i-Mompel, P. *et al.* decoupleR: ensemble of computational methods to infer biological activities from omics data. *Bioinformatics Advances* **2**, vbac016 (2022).
88 Malagoli Tagliazucchi, G., Wiecek, A. J., Withnell, E. & Secrier, M. Genomic and microenvironmental heterogeneity shaping epithelial-to-mesenchymal trajectories in cancer. *Nature communications* **14**, 789 (2023).
89 Finan, C. *et al.* The druggable genome and support for target identification and validation in drug development. *Science translational medicine* **9**, eaag1166 (2017).
90 Jin, S. *et al.* Inference and analysis of cell-cell communication using CellChat. *Nature communications* **12**, 1088 (2021).
91 Kristensen, M. W. *et al.* Vol. 99 265-268 (Wiley Online Library, 2021).
92 Emmaneel, A. *et al.* PeacoQC: Peak-based selection of high quality cytometry data. *Cytometry Part A* **101**, 325-338 (2022).

Figure 1

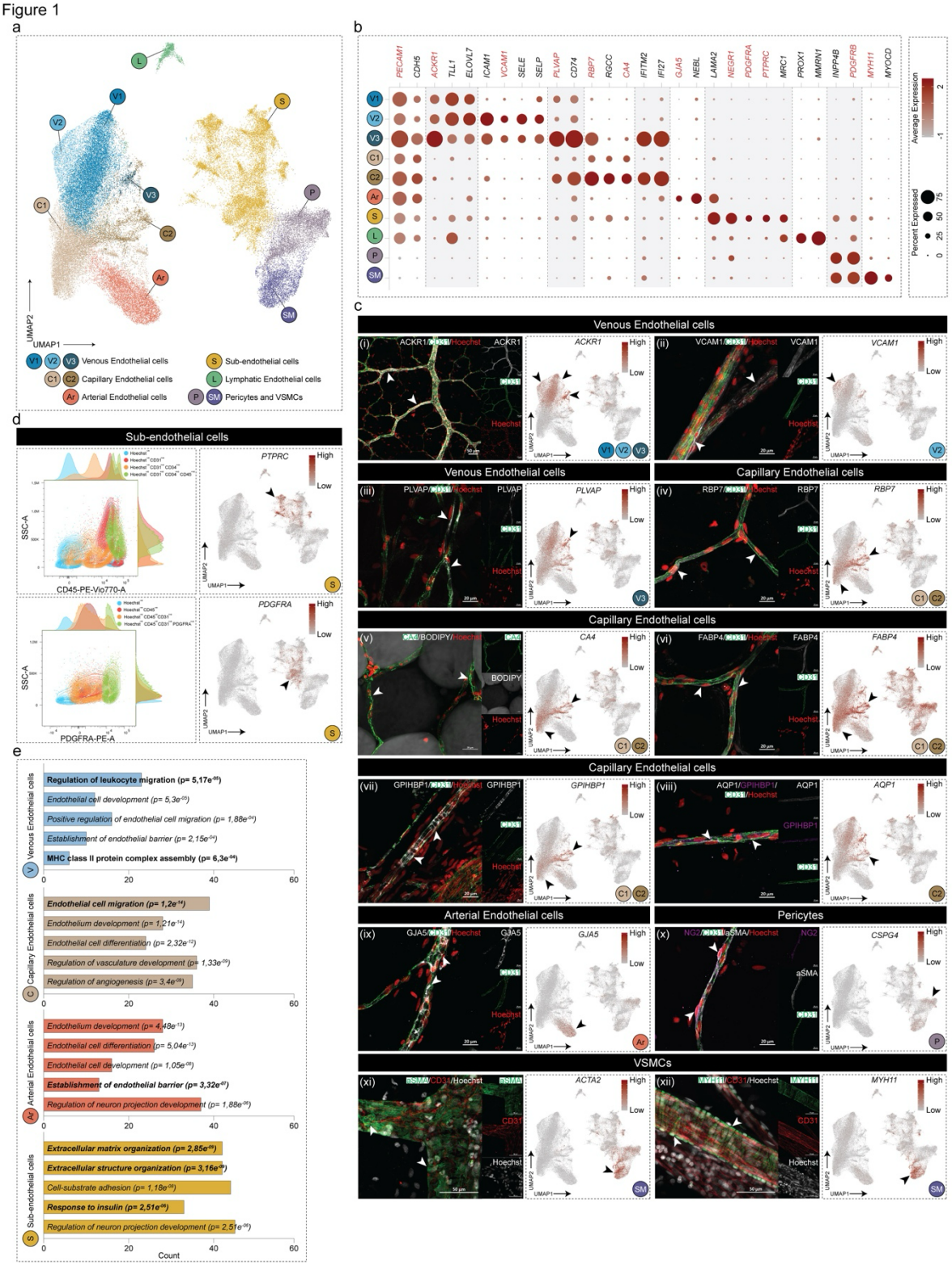

Figure 2

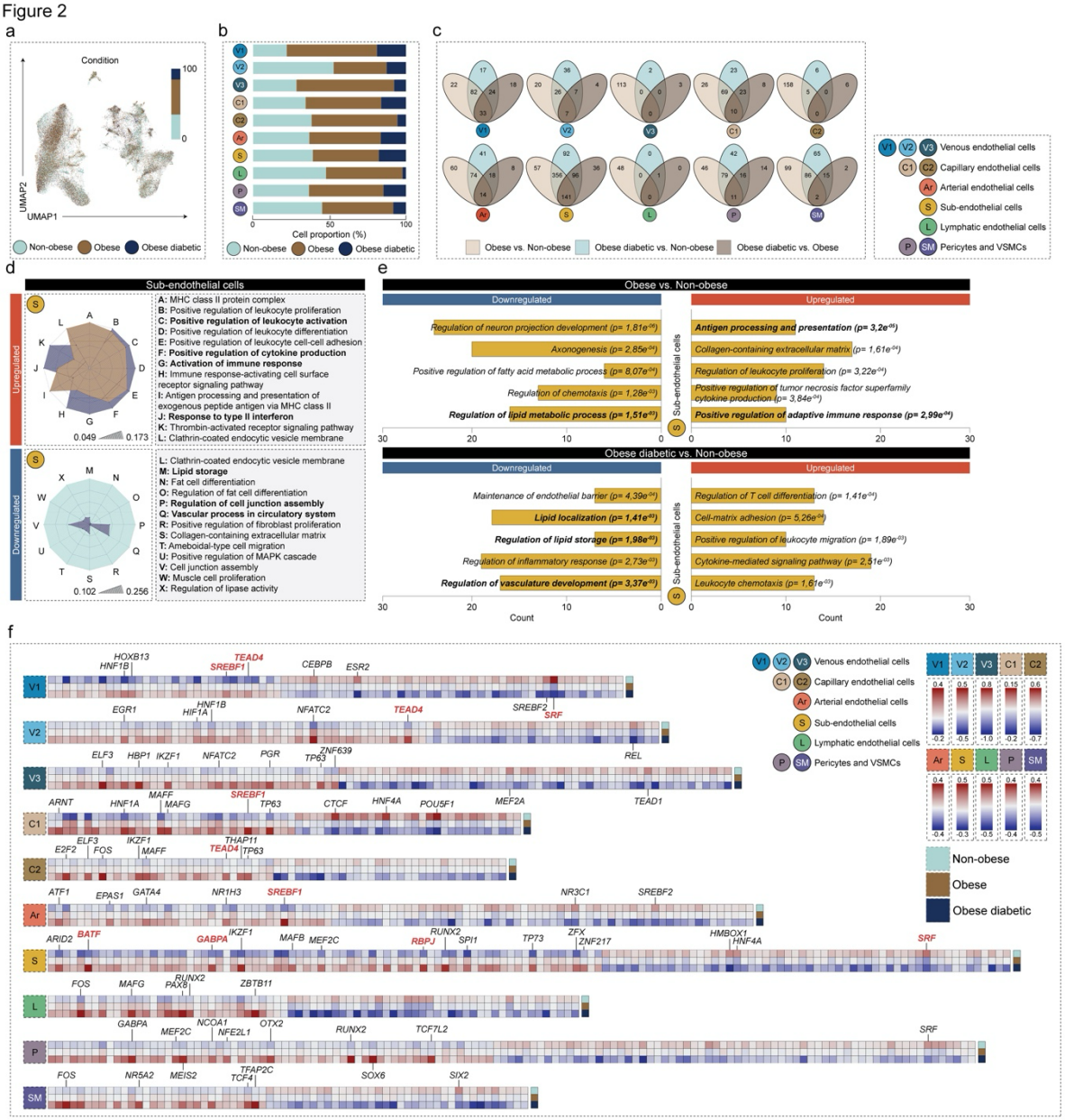

Figure 3

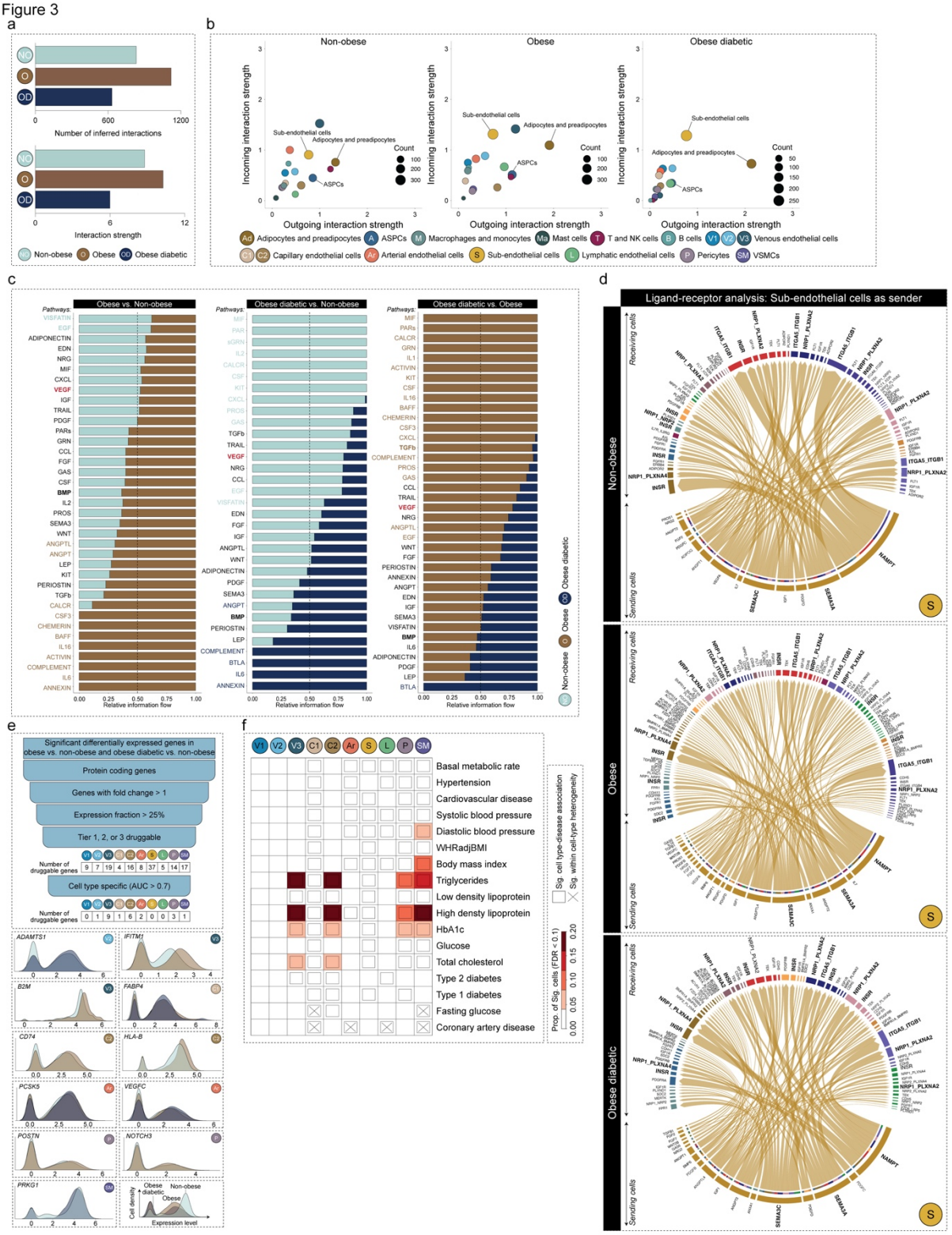

Figure 4

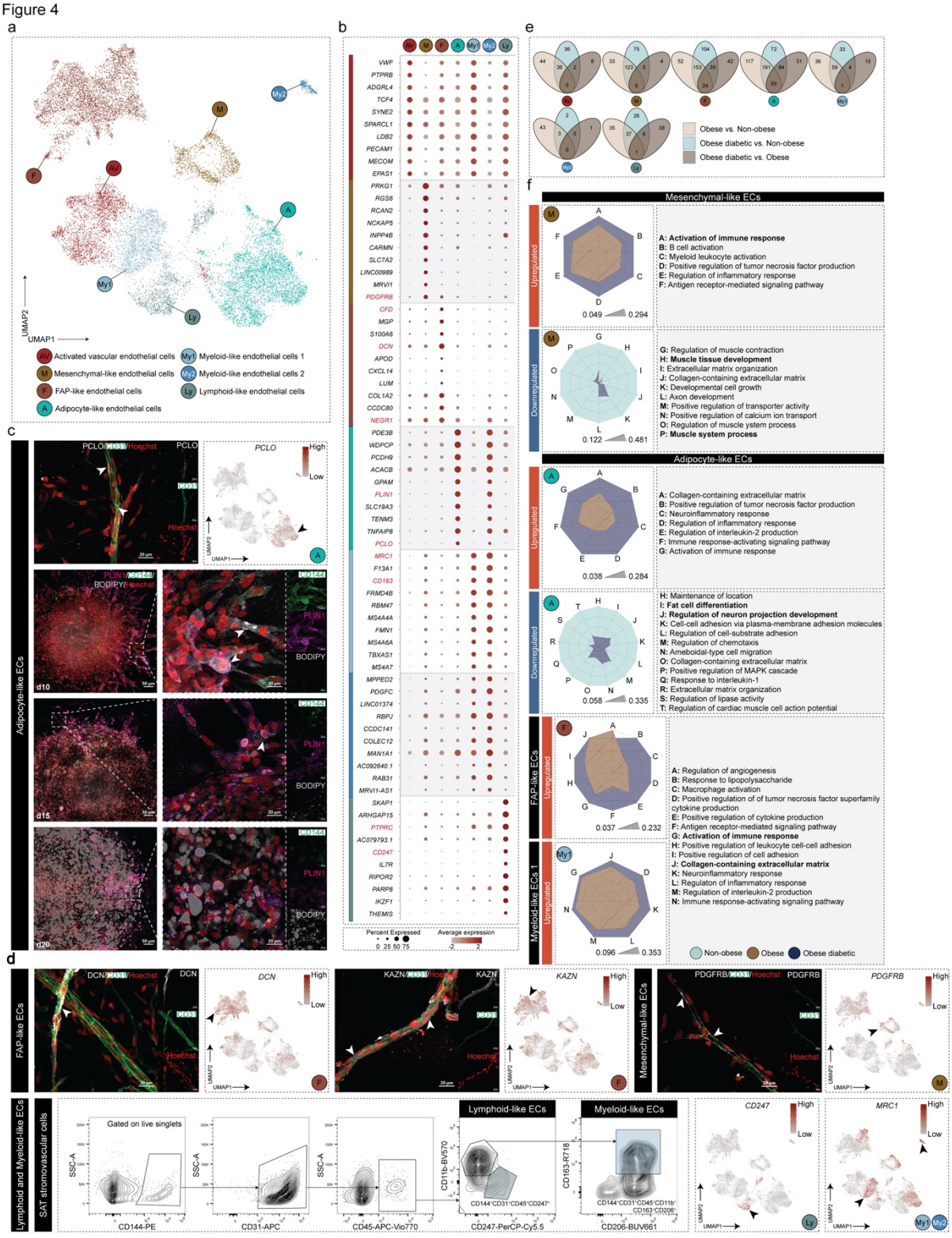

Extended Data Figure 1

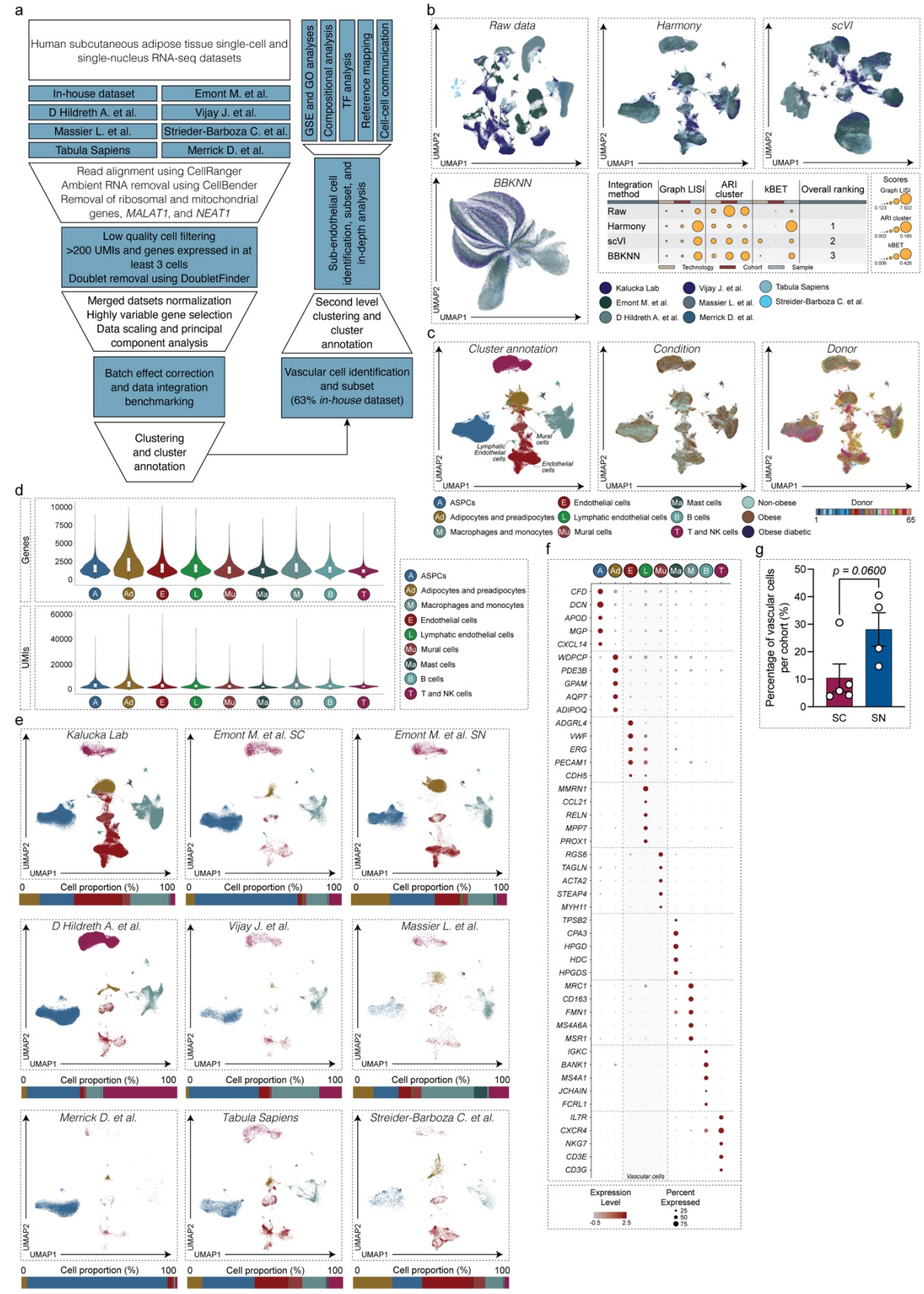

Extended Data Figure 2

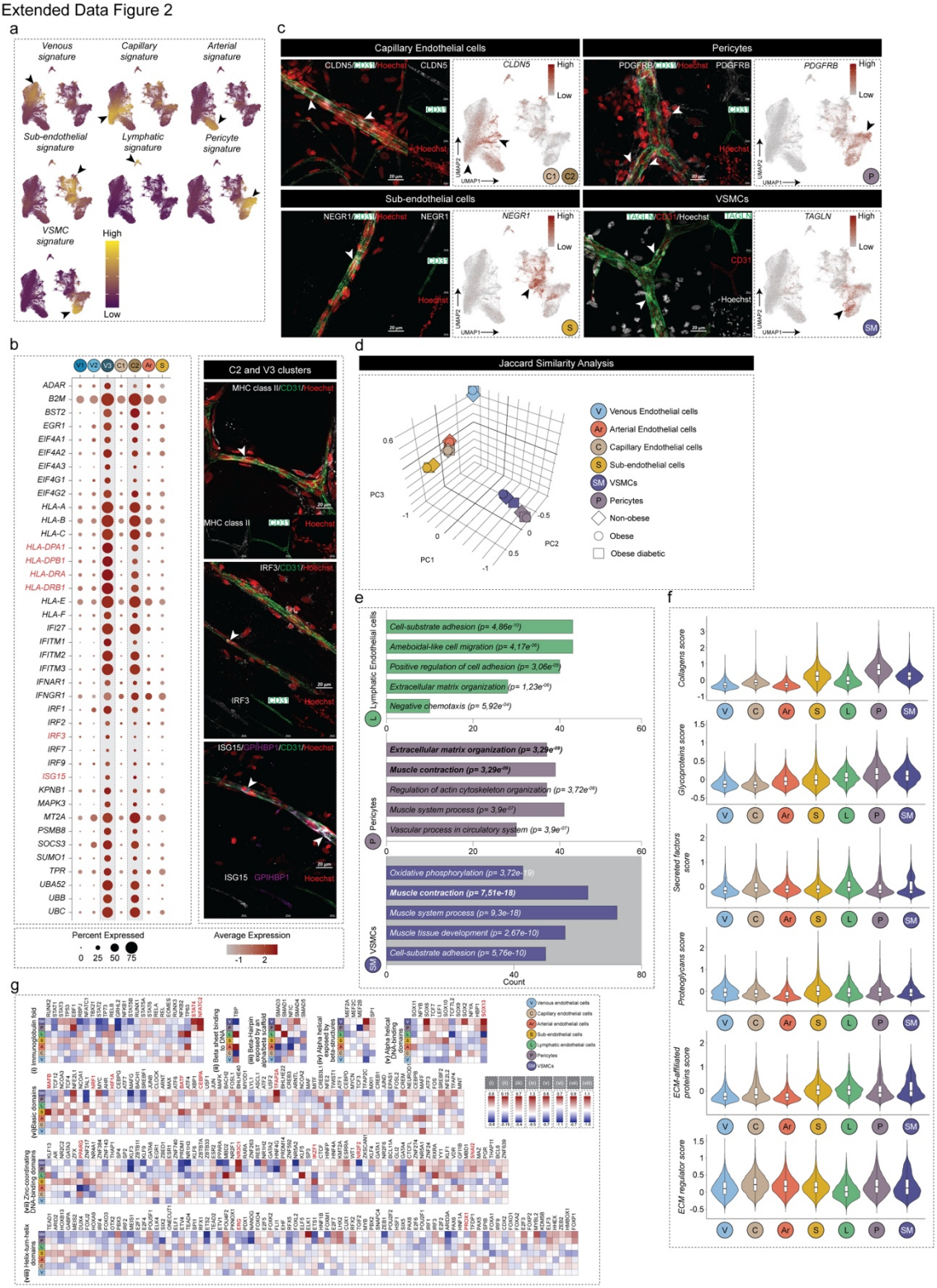

Extended Data Figure 3

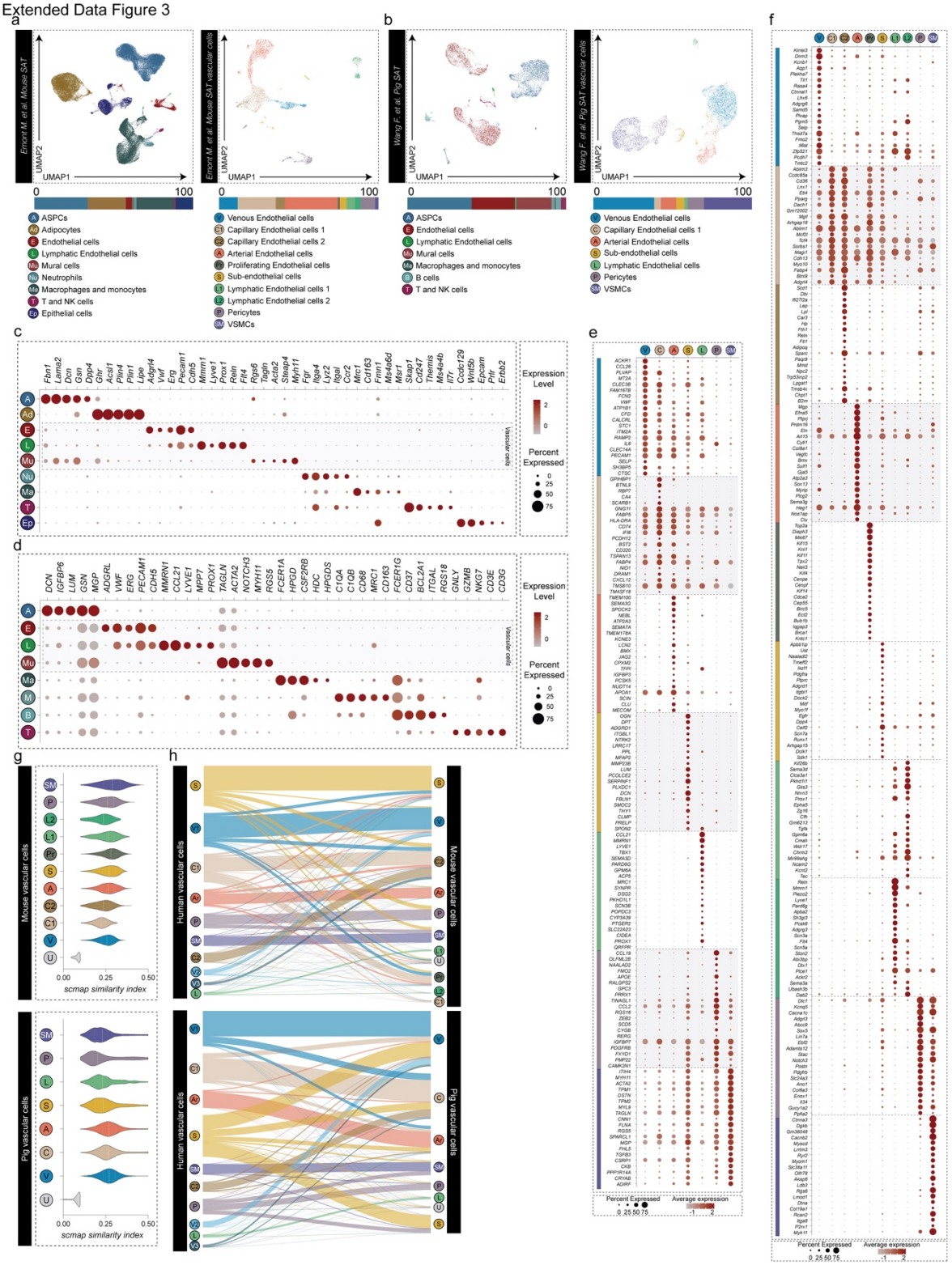

Extended Data Figure 4

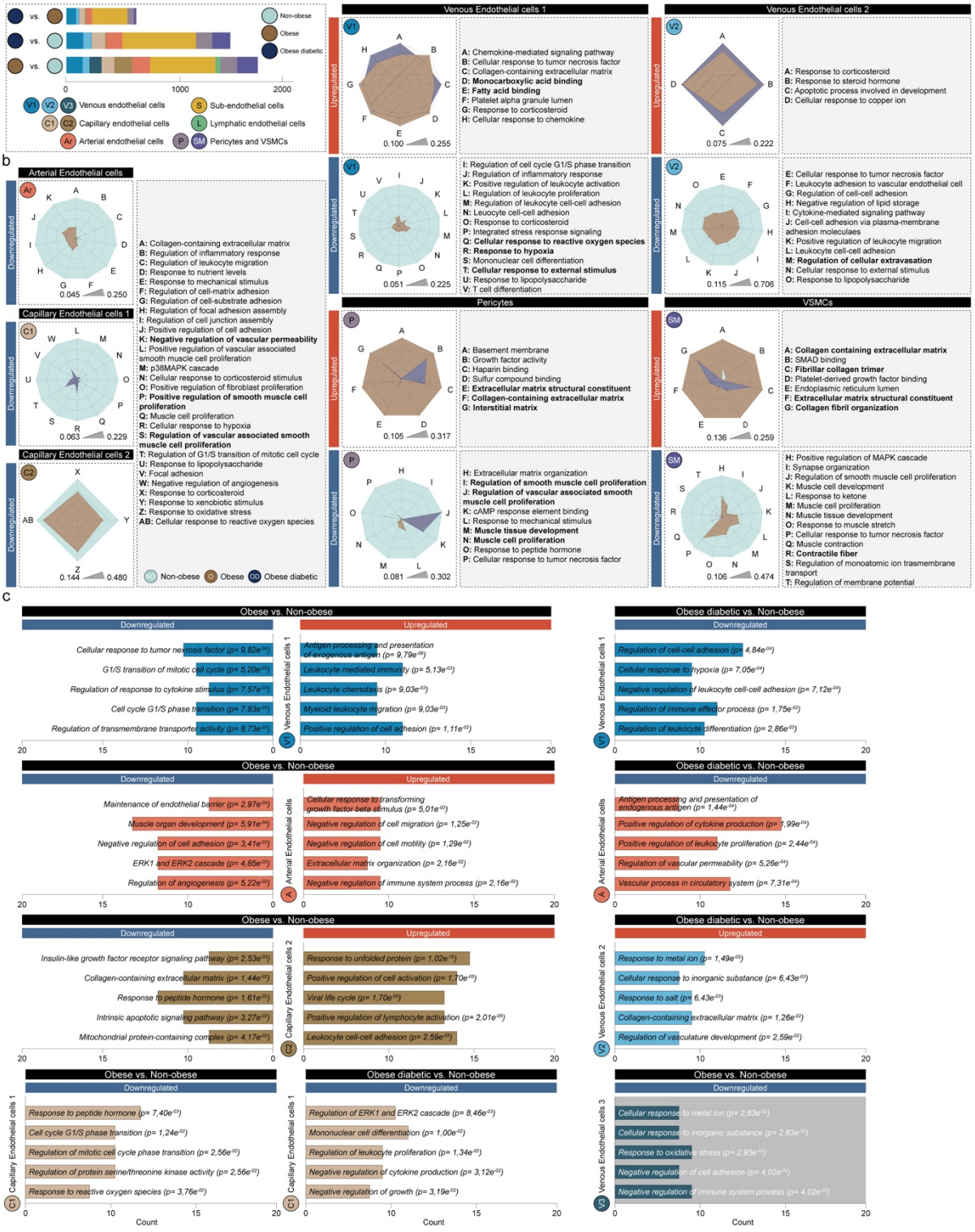

Extended Data Figure 5

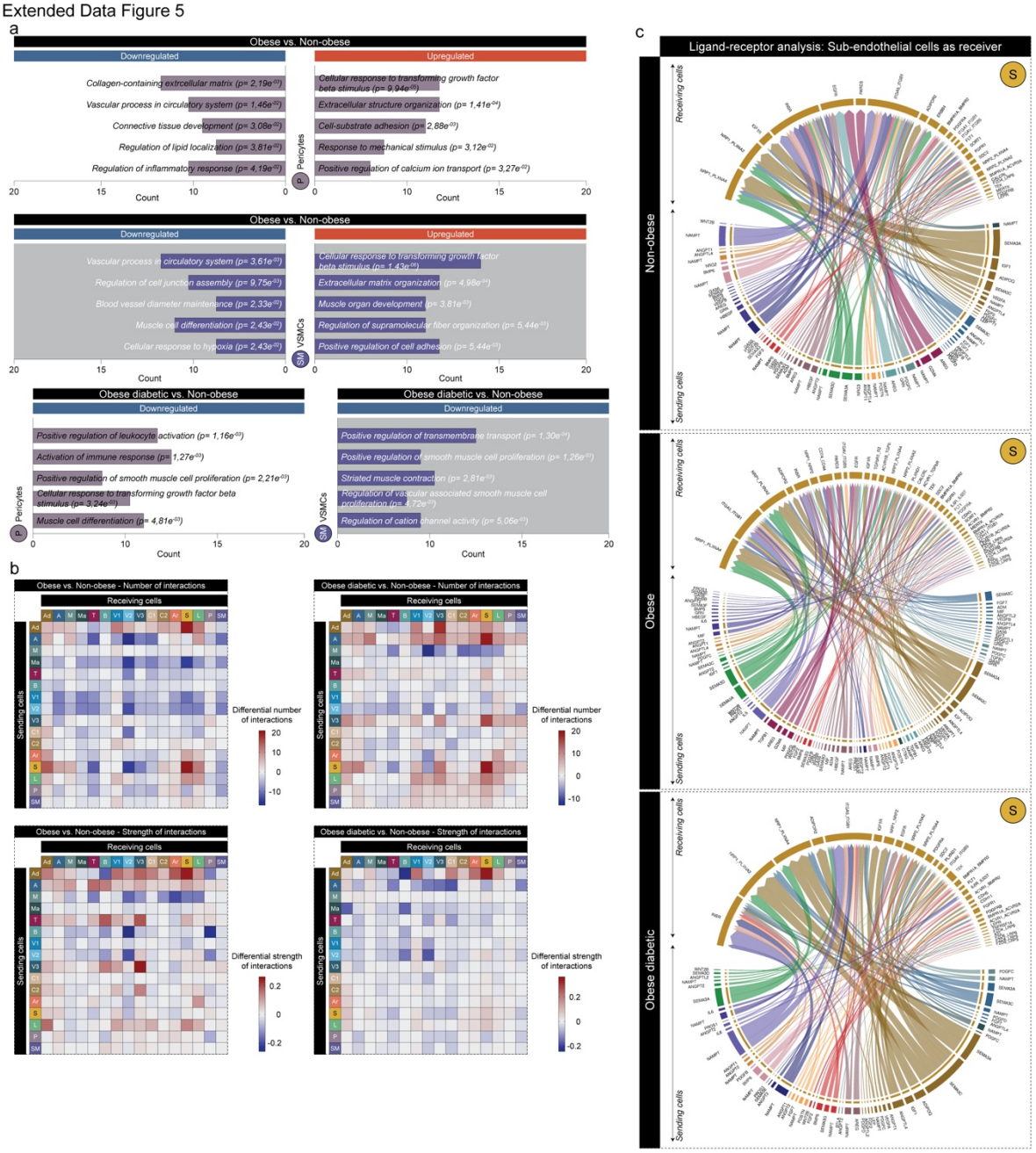

Extended Data Figure 6

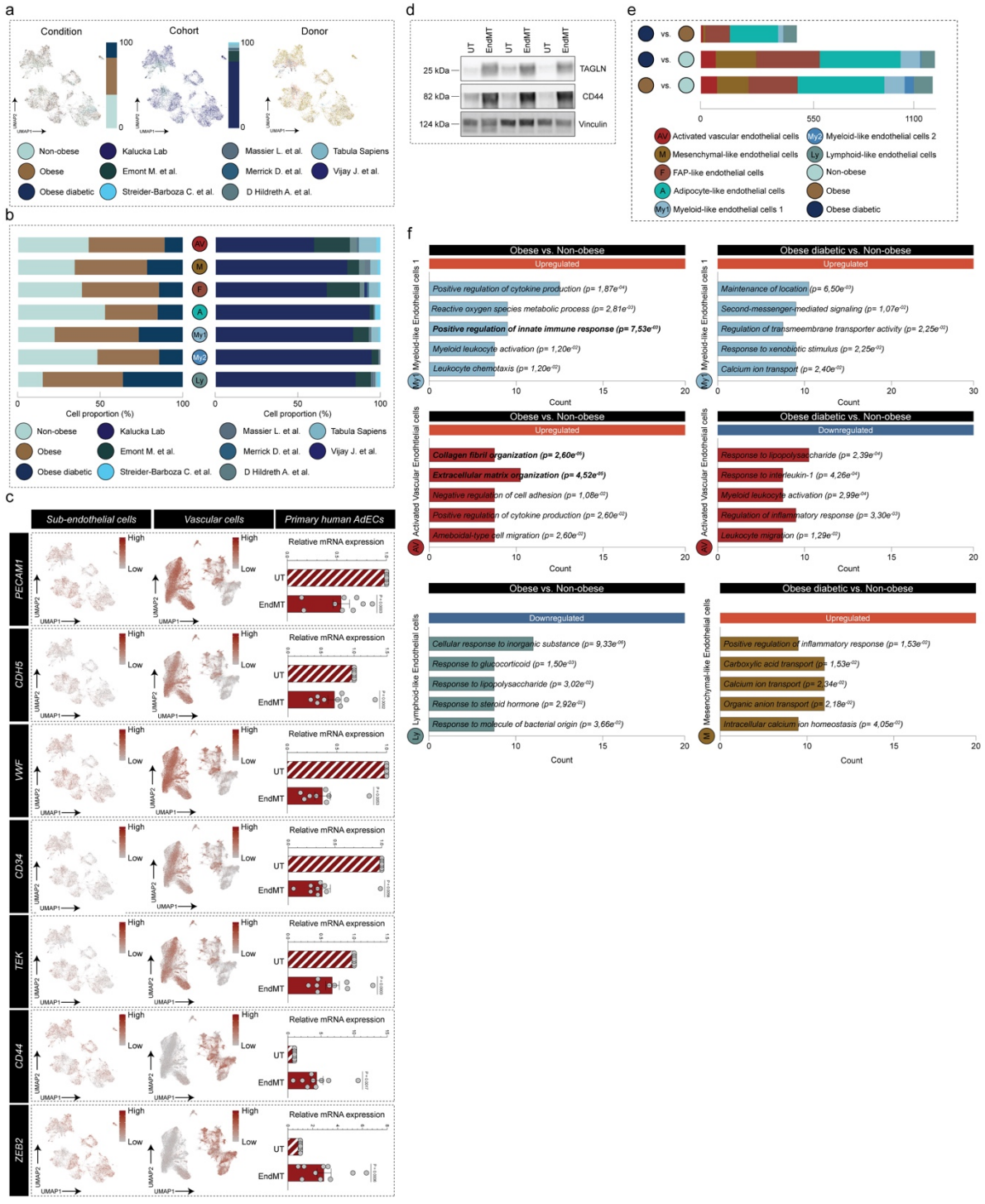

Extended Data Figure 7

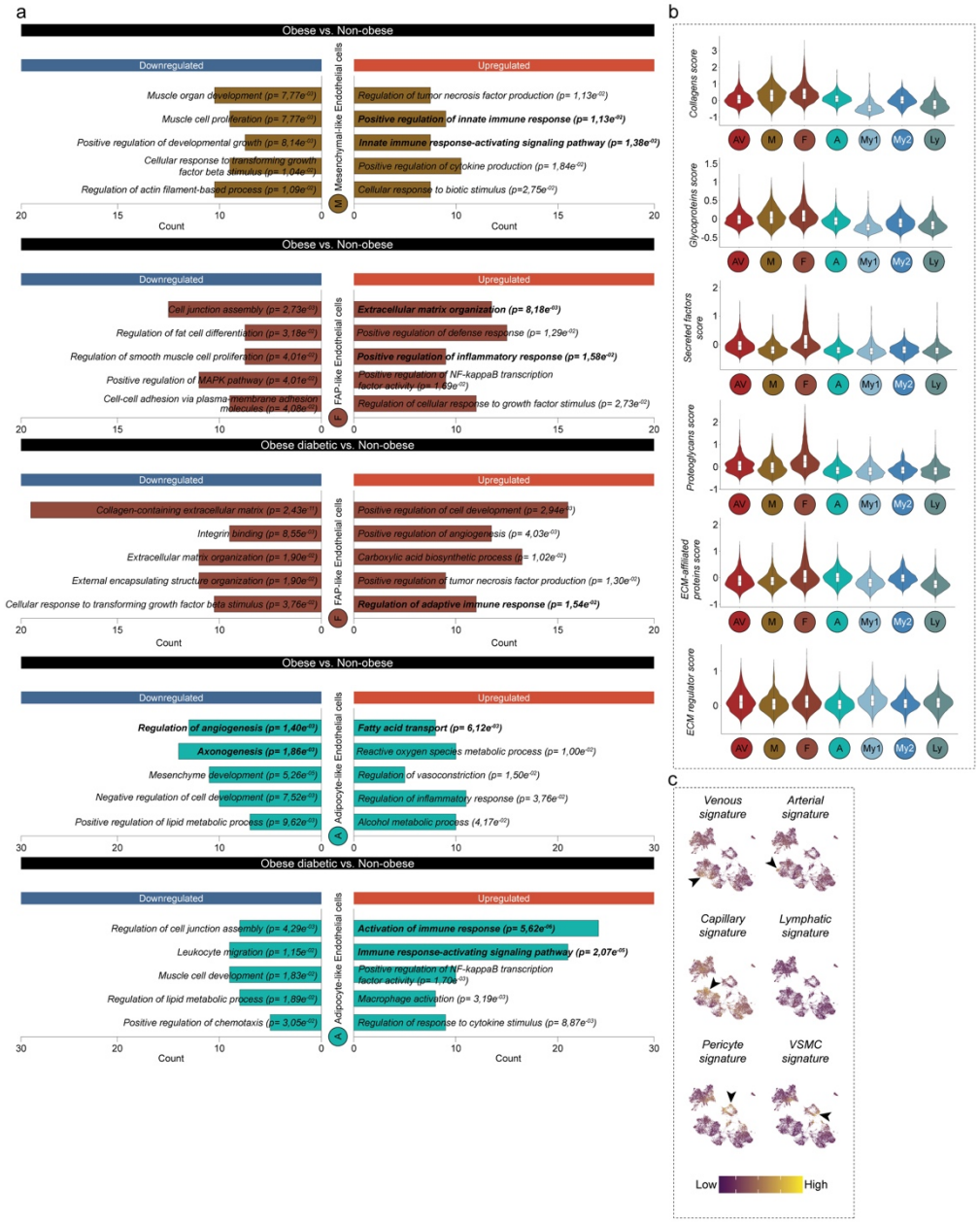

Extended Data Figure 8

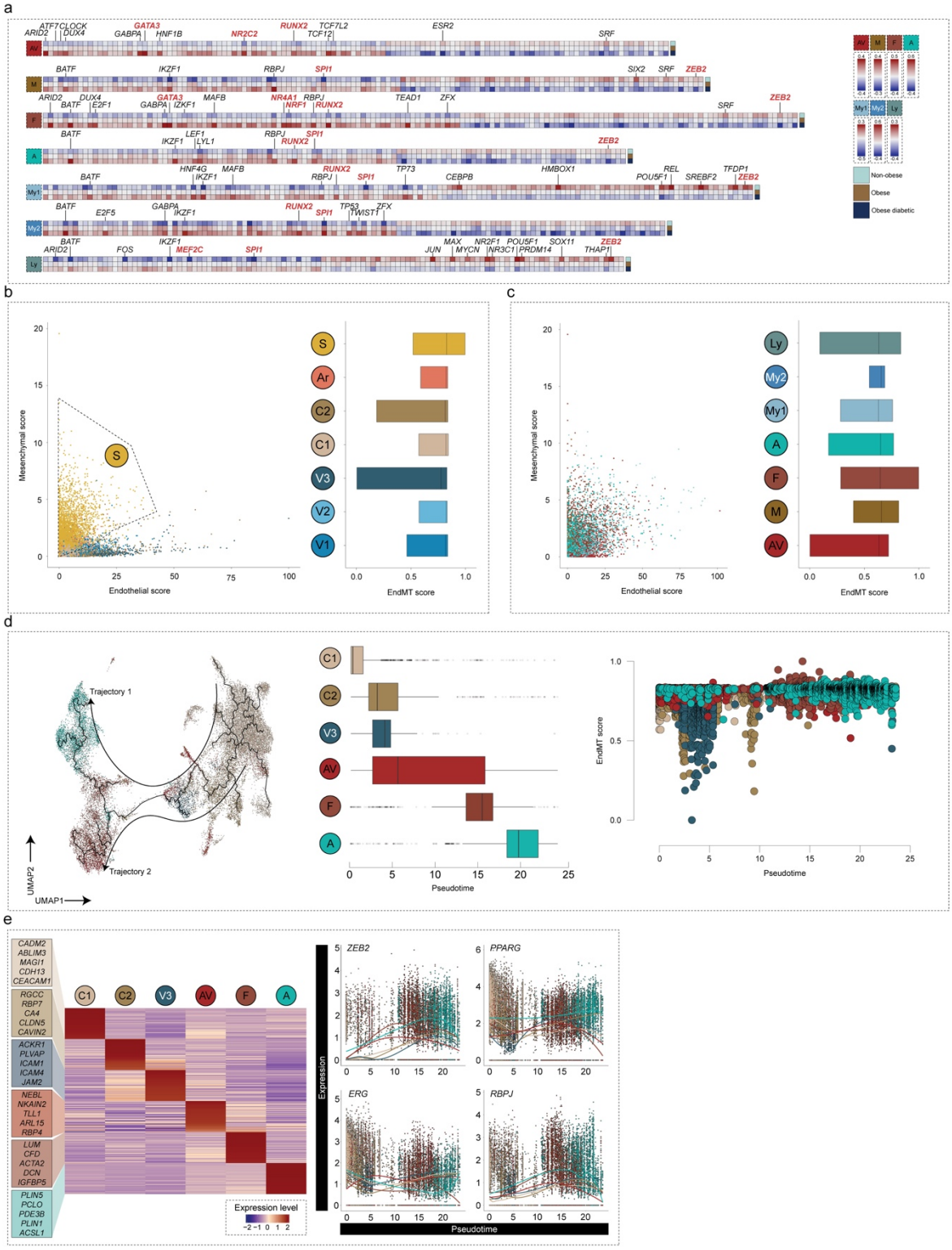

Supplementary Figure 1